INVESTIGATION OF GATE LEAKAGE CURRENT IN NITROGEN IRRADIATED $Al_xGa_{1-x}N$/GaN HETEROSTRUCTURES

THESIS

Rose E. May, Captain, USAF

AFIT/GNE/ENP/11-M14

DEPARTMENT OF THE AIR FORCE
AIR UNIVERSITY

AIR FORCE INSTITUTE OF TECHNOLOGY

Wright-Patterson Air Force Base, Ohio

AFIT/GNE/ENP/11-M14

INVESTIGATION OF GATE LEAKAGE CURRENT IN NITROGEN IRRADIATED $Al_xGa_{1-x}N$/GaN HETEROSTRUCTURES

THESIS

Presented to the Faculty

Department of Engineering Physics

Graduate School of Engineering and Management

Air Force Institute of Technology

Air University

Air Education and Training Command

In Partial Fulfillment of the Requirements for the

Degree of Master of Science in Nuclear Engineering

Rose E. May

Captain, USAF

March 2011

AFIT/GNE/ENP/11-M14

INVESTIGATION OF GATE LEAKAGE CURRENT IN NITROGEN IRRADIATED $Al_xGa_{1-x}N$/GaN HETEROSTRUCTURES

Rose E. May
Captain, USAF, B.S., M.S.

Approved:

_____	_____
James C. Petrosky, PhD (Chairman)	Date
_____	_____
LTC John W. McClory (Member)	Date
_____	_____
Robert L. Hengehold, PhD (Member)	Date

AFIT/GNE/ENP/11-M14

Abstract

Due to commercial and government interest in devices capable of functioning in high-power, high-frequency space applications, inherently radiation tolerant AlGaN/GaN devices have been under study in recent years. The 2-degree electron gas (2DEG) created at the AlGaN/GaN interface is affected by electron trapping in AlGaN surface states. Passivation of the AlGaN surface by silicon nitride (Si_3N_4) prevents this electron trapping and enhances the 2DEG. However, this passivation also increases gate leakage currents, an undesirable effect leading to device failure. It has been shown that thermionic trap-assisted tunneling (TTT) currents can account for some of the effects observed in the leakage model. This study sought to uncover additional details about the current leakage mechanisms by introducing displacement damage as close to the Si_3N_4/AlGaN interface as possible.

The effects of ion irradiation damage at or near the Si_3N_4/AlGaN interface gate leakage current were investigated for three thicknesses of Si_3N_4 passivation (200Å, 500Å, and 1200Å). Silicon nitride-passivated AlGaN/GaN samples were irradiated at room temperature with 15-50 keV nitrogen ions. Nitrogen was chosen to minimize changes to chemistry at the interface. Hall measurements were made to determine mobility and 2DEG carrier density. C-V measurements provided insight into charge type and location and effects on the band structure. Baseline pre-irradiation measurements were compared to the irradiation results to determine the types and amounts of damage done in the

device. A baseline with no Si_3N_4 was used to compare the effects of irradiation on passivation.

Post-irradiation C-V measurements showed a greater than 50% decrease in capacitance and an average negative threshold voltage shift of 3 V, which persisted for over a week in the passivated samples but not in the unpassivated sample. Post-irradiation Hall measurements showed decreases in mobility for both passivated and unpassivated samples. Carrier concentration decreased for passivated samples but increased for the unpassivated sample.

Acknowledgements

There are many people I would like to acknowledge and thank for the help and support they provided me while I was pursuing this graduate degree. My thesis advisor and committee members, Dr. James Petrosky, LTC John McClory, and Dr. Robert Hengehold, were instructive, positive, and patient as I struggled to understand the phenomena I was researching. The AFRL staff was instrumental in providing the samples for me to work with as I repeatedly returned for wire bonding and soldering. Dr. Daniel Felker and Mr. Eric Taylor provided time, equipment, and expertise as I characterized my samples before and after irradiation. Personnel at the SNL Ion Beam Laboratory also provided time, equipment, and expertise, leading me to expand my initially planned procedure. This resulted in the collection of additional data that resulted in a better understanding of the phenomena involved. Finally, I would like to thank my family for their patience and long-suffering as I pursued my graduate education.

Table of Contents

Page

List of Figures

Figure Page

List of Tables

INVESTIGATION OF GATE LEAKAGE CURRENT IN NITROGEN IRRADIATED $Al_xGa_{1-x}N$/GaN HETEROSTRUCTURES

I. Introduction

A. Background

AlGaN/GaN

Gallium nitride (GaN), a III-V semiconductor material, has a number of properties that make it appealing for use as a semiconductor material in radiation environments. It has a wider band gap, higher melting point, higher breakdown voltage, and lower dielectric constant than silicon and gallium arsenide. Some of the attributes are listed in Table 1 [1], [2]. These properties, in addition to its intrinsic radiation tolerance, indicate that GaN will likely function very well in high power, high frequency space applications, as well as in other particularly rugged environments [1], [3], [4]. However radiation-induced gate leakage currents in aluminum gallium nitride ($Al_{0.27}Ga_{0.73}N$)/GaN devices limit performance. Identifying the mechanisms behind the gate leakage currents following irradiation will allow needed design and engineering improvements to the devices, which will result in appropriately radiation hardened systems for vital civilian and military applications.

Table 1. Comparison of some basic parameters of GaN, Si, and GaAs

Material	Band gap	Thermal conductivity	Power switching capability
GaN	3.49 eV	Up to 1.97 W/cm-K	30.6 W/mm @ 8 GHz
Si	1.12 eV	1.30 – 1.45 W/cm-K	0.6-0.8 W/mm [5]
GaAs	1.43 eV	0.55 W/cm-K	1 W/mm @ 10 GHz

As a result of AlGaN/GaN lattice mismatch, strain, and inherent piezoelectric characteristics, a 2-D electron gas (2DEG) forms at the interface between the AlGaN and the GaN [4]. The 2DEG exists in the quantum well formed between the conduction band edges of the AlGaN/GaN interface and the GaN, illustrated as the "channel" in Figure 1 and as such can be switched off and on very quickly, on the order of GHz. Because of this high-speed switching capability, AlGaN/GaN devices easily lend themselves to use in high frequency applications.

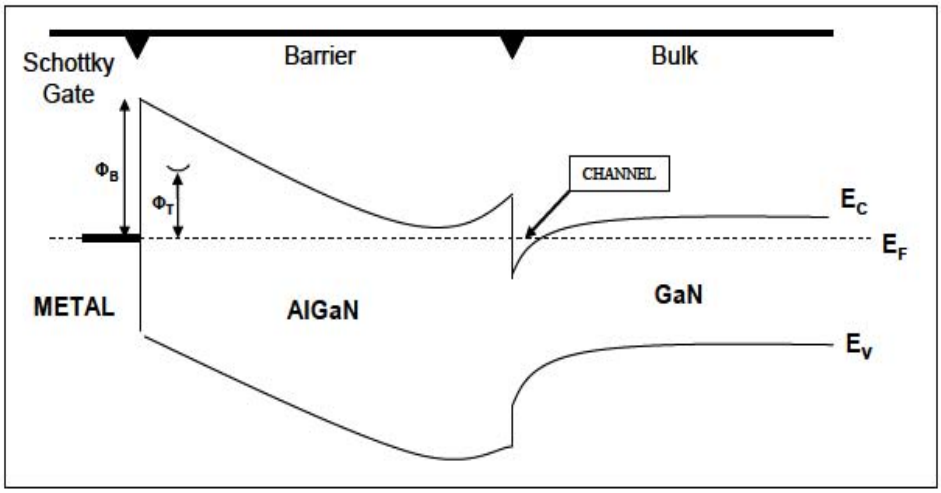

Figure 1. Band diagram of the AlGaN/GaN heterostructure [6]

Passivation & effects on gate leakage

One drawback of AlGaN is that bare AlGaN develops a negative sheet charge at the air/AlGaN interface as electrons get trapped by ionized donor sites [7]. This increasingly negative sheet charge counters the polarization at the interface and adversely affects the formation of the 2DEG just below the AlGaN. Applying a passivation layer, such as Si_3N_4, prevents this negative sheet charge from forming and increases the carrier concentration in the 2DEG [8]. A Si_3N_4 passivation layer, however, also increases gate

leakage current, which has been under investigation for over ten years [9]. Various theories, including Schottky barrier lowering, thermionic emission and thermionic field emission through the Schottky barrier, trap-assisted tunneling through the Schottky barrier, and surface leakage at the Si_3N_4/AlGaN interface, have been proposed to explain the increased gate current.

B. Focus of research/problem statement

This study seeks to identify gate current mechanisms consistent with the thermionic trap-assisted tunneling (TTT) model by damaging the passivation layer as close to the passivation/AlGaN interface as possible using low-energy nitrogen ions. The nitrogen ions will produce displacement damage, which is expected to facilitate TTT through the Schottky junction providing enough data to validate the thermionic TTT model.

C. Hypothesis

Gate leakage current is dominated by TTT through the Schottky barrier. Creating additional traps at the Si_3N_4/AlGaN interface will increase leakage currents and make them more easily identified through changes in capacitance, mobility, and carrier concentration.

D. Approach & scope

- Use devices with different thicknesses of Si_3N_4 passivation as well as unpassivated devices. The Si_3N_4 thicknesses will be 200 Å, 500 Å, and 1200 Å.
- Use N^+ to create damage. The ions will neutralize within the first few nanometers of the Si_3N_4 and therefore cause primarily displacement damage.

- Use low energy ions in order to deposit most of the energy in the Si_3N_4 or at the Si_3N_4/AlGaN interface. Based on results from TRIM models, the ion energies will be 15 keV at an incident angle of 45 degrees for the unpassivated and 200Å Si_3N_4 samples, 20 keV incident normal to the surface for the 500Å passivated devices, and 50 keV incident normal to the surface for the 1200Å passivated devices. 15 keV at a 45 degree angle will be equivalent to an energy of 10 keV normal to the surface, which may be too low an energy for the beam line.
- Use a fluence of N^+ equivalent to 10^{16} 1 MeV electrons/cm^2 for comparison with other research being done at AFIT on devices from the same wafers.
- Use room temperature capacitance-voltage (C-V), current-voltage (I-V), and Hall measurements post-irradiation to characterize the effects of the irradiation on the electrical properties and charge carriers heterostructures.

II. Theory

A. Device Function

As described in [2] and [4], a 2DEG is formed due to the inherent piezoelectric properties of GaN and AlGaN and the lattice size mismatch when the AlGaN is grown on the GaN. As such, the device is always on and in a state of accumulation unless a negative voltage sufficient to deplete the channel is applied to the gate. Unpassivated AlGaN develops a negative surface sheet charge that diminishes the 2DEG, likely due to electron-capturing surface states [4]. Passivating the AlGaN surface (e.g. with Si_3N_4) neutralizes these surface states, prohibiting electron capture, and actually enhancing the 2DEG [10]. Passivating with Si_3N_4 also increases gate currents which affect the voltage required for proper transistor operation and consequently power consumption, [10]. The gate currents must be reduced in order to mitigate the corresponding power consumption and shift in required voltage, especially for those devices used in space or other environments where it is difficult to make repairs.

B. Radiation damage

Radiation can cause two types of damage: displacement and ionization. Displacement damage is caused by elastic collisions knocking atoms out of lattice positions and creating vacancies and interstitials. Displacement damage creates long-term defects, which may manifest themselves as traps that act as centers for hopping transport, allowing carriers to tunnel through the Schottky barrier at the gate metal/AlGaN interface, resulting in increased leakage currents.

Ionization is a secondary effect of displacement damage. Electron-hole pairs are created by the displaced atoms, and the local electric field causes the separation and movement of these charged particles. The electrons, having a higher mobility, are swept out of the material leaving the holes behind [1]. The lower mobility of the holes is partially due to their larger effective mass. Due to this lower mobility, the holes are more susceptible to Coulombic forces and defects in the lattice, and therefore, become trapped. The positive charge due to the trapped holes increases, changing the electric field and, therefore, V_{th} by attracting electrons to the interface.. This then requires an increasingly negative gate bias to deplete the channel.

While GaN is inherently more "radiation hard" than silicon, the effects of radiation on GaN devices must be well-understood for them to be used confidently in high-frequency, high-power space-based applications. [11] and [12] have measured increased gate currents due to neutron irradiation. Radiation induced gate leakage is attributed to increases in trap-assisted tunneling (TAT), based on research and model fitting by [13], [2] achieved an "excellent fit" to the thermionic trap-assisted tunneling (TTT) model using I-V and current-temperature (I-T) data from devices irradiated by high energy neutrons.

Proton irradiation also increases gate leakage current [14]. The absolute value of threshold voltage ($|V_{th}|$), Schottky barrier height, and effective donor doping concentration all decreased with proton irradiation (i.e. V_{th} *less* negative). The changes were attributed to gallium vacancies or complexes—thought to be acceptor defects—compensating for donors [2].

C. Leakage models for the heterojunction bipolar transistor

Gray [2] proposed 3 primary current paths for gate leakage in heterojunction bipolar transistors (HBTs) as shown in Figure 2:

1. Lateral surface current, possibly due to conductive residue or defect hopping, across unpassivated AlGaN from gate to drain
2. From the gate through the Schottky barrier and through the AlGaN bulk to the drain
3. Through the Schottky barrier and the AlGaN to the 2DEG to the drain

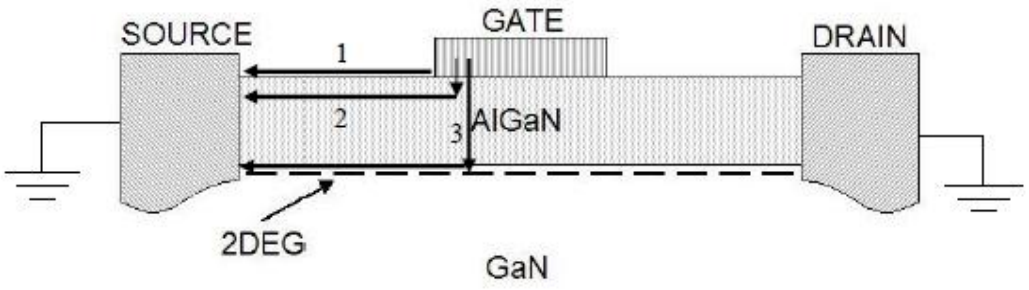

Figure 2. Potential current paths through an HBT [2]

[2] also presented six methods of carrier transport across the Schottky barrier the first three of which are shown in Figure 3:

a. Thermionic emission: due to sufficient thermal energy, electrons pass over the Schottky barrier
b. Thermionic field emission: through the top/thin part of the Schottky barrier
c. Field emission (direct tunneling): through the bottom/thick part of the Schottky barrier
d. TAT through the Schottky barrier: 2 paths
    i. Field emission/direct tunneling, negligible at T > 500 K because of the width of the Schottky barrier [2]

ii. TAT via deep traps "spread over an energy band" (or in simpler model, "a single trap energy within the AlGaN band gap") in the Schottky barrier, dominates at T < 500 K [13]

e. Thermionic emission + Schottky barrier thinning

f. Generation-recombination

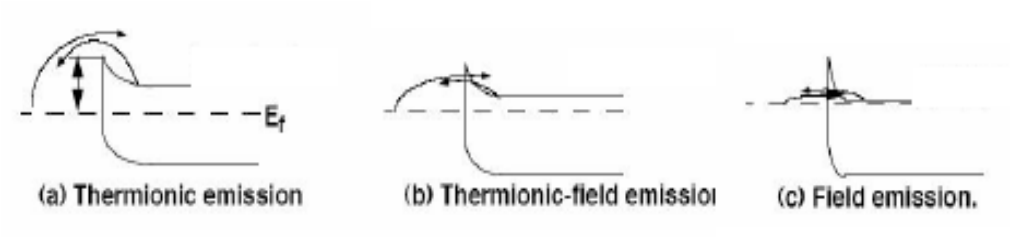

Figure 3. (a), (b), and (c) illustrate three types of transport across the Schottky barrier. [2].

Despite an expected high density of surface defects on an unpassivated AlGaN surface, [2] ruled out AlGaN surface current as the dominant current path due to the gate current saturating for $V_g > V_{th}$. Due to the direction of the electric field (perpendicular to the gate), electron travel parallel to the AlGaN surface is unlikely and "not a viable current path" [2]. The electrons are more likely to travel vertically through the AlGaN to the 2DEG than horizontally to the drain. However, in this research, the use of a passivation layer and low-energy positive ions to create defects in the passivation layer and interface could cause enough defects for the lateral surface leakage current across the AlGaN to become dominant.

The other two paths involve tunneling through the Schottky barrier, the primary interest of this research. According to [15], the electric field line curvature near the gate edges is reduced because of "the presence of a high negative net charge at the AlGaN/passivation interface [which] introduces a depletion region along the surface

between the gate and source/drain." Therefore, angular tunneling away from the gate toward the drain is negligible, and the primary current path through the Schottky barrier is normal to the gate/AlGaN interface. Additionally, the TTT model provides a better fit to data than a direct tunneling model. Once in the AlGaN, the electrons could tunnel through the AlGaN to the drain or to the 2DEG. Again, due to the direction of the electric field, the likely path is through the AlGaN to the 2DEG, then to the drain. However, the damage caused by the nitrogen ions may significantly increase the probability of tunneling across to the drain without reaching the 2DEG first.

D. Measurements

Purpose of C-V measurements

A high frequency (1MHz) C-V measurement will yield capacitance with the underlying semiconductor in both accumulation and inversion. In the case of an AlGaN/GAN device, the capacitance measured when the GaN is in accumulation is the capacitance of the AlGaN, equivalent to C_{ox} in a MOS device, and under inversion the capacitance is the series sum of C_{AlGaN} and the GaN semiconductor depletion layer capacitance, C_j [16]. Under strong inversion, the minimum capacitance is given by

$$C_{\min} = \frac{\varepsilon_{AlGaN}}{d + \frac{\varepsilon_{AlGaN}}{\varepsilon_s} W_{\max}} = \frac{\varepsilon_{AlGaN}}{d + \frac{\varepsilon_{AlGaN}}{C_j}} \text{ [16].} \quad (1)$$

In MOS structures, a persistent negative ΔV_{th} shift is attributed to "long-term trapping of net positive charge in the oxide layer" [17]. Similarly, threshold voltage in the AlGaN/GaN structures is expected to shift more negative due to the presence of trapped holes formed by ionizing radiation in the Si_3N_4 and because of the eventual adoption of

the +2 charge state by the implanted nitrogen atoms. The additional positive charge will attract more electrons to the 2DEG requiring a greater negative bias to close the channel. C-V measurements will be made by sweeping the applied bias from inversion to accumulation (negative to positive values) as recommended by [18], which allows charge carriers to re-establish equilibrium after each change in voltage.

Previous research by [19] measured voltage shifts in the transition region of the C-V relationship (voltage shift) but only small changes in the accumulation and depletion capacitances. [19] states that "irradiated MOS structures retain their basic capacitance behavior even after high [proton] irradiation...." This is shown in Figure 4, taken from [17]. There is a negative voltage shift immediately after irradiation with the same shape as the pre-irradiation curve. Over time the curve shifts back toward positive voltage while its shape stretches out to indicate the formation of radiation-induced interface traps [17].

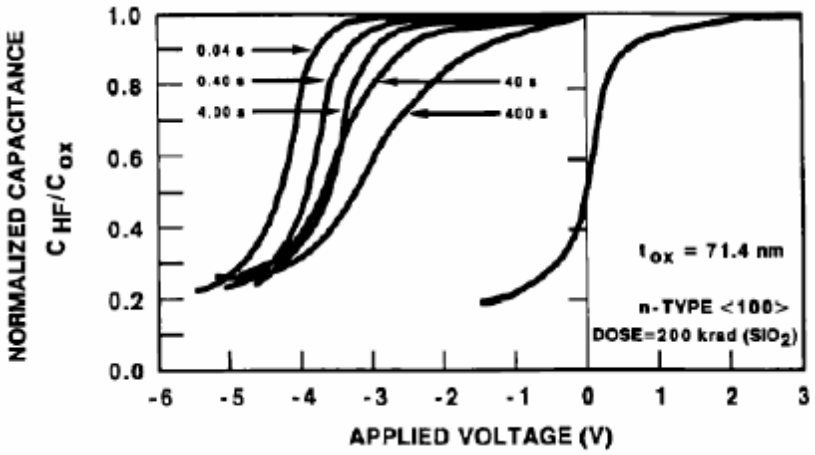

Figure 4. This figure illustrates normalized capacitance vs. applied gate voltage of a MOS capacitor before and over time after irradiation [17].

The "stretch" in the slope of the C-V curve between accumulation and inversion can be used as a measure of time-dependent radiation-induced interface trap formation [17] according to the equation

$$\Delta N_{it} = C(\frac{\Delta V_{it}}{q}), \quad (2)$$

where C is the AlGaN capacitance, and ΔV_{it} is the shift in voltage at the minimum and maximum capacitance points in the linear part of the depletion region of the pre- and post-irradiation C-V curves. The C-V curve stretched out because acceptor traps above the Fermi level in the GaN bandgap are neutral. As the applied voltage reaches inversion, the acceptor traps begin to move below the Fermi level, trapping electrons, requiring greater applied voltage to reach the same capacitance as without them. An increase in capacitance is a result of an increase in doping level in the structure as shown in Figure 5. However, the addition of the nitrogen from the irradiation accounts for only about 2×10^{-12} of the total number of atoms in the Si_3N_4 and, therefore, will be insufficient to show a capacitance shift.

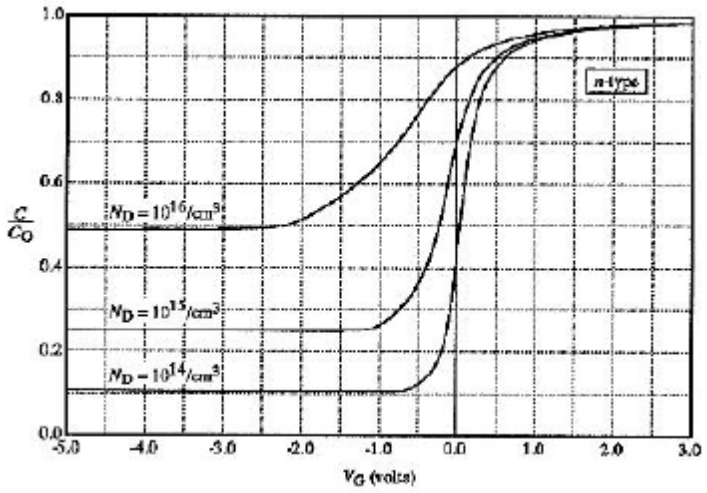

Figure 5. Doping dependence of MOS capacitor high frequency C-V characteristics [20]

Purpose of I-V measurements

Changes in the forward-bias slopes of gate-to-ohmic I-V curves may indicate a change in current mechanism (diffusion vs. recombination) [16]. Forward bias current remains low until the applied gate voltage becomes greater than the Schottky barrier height and then increases rapidly. This occurs around 1 V in GaN-based devices. Changes in forward bias current between 0 and 1 V would indicate damage at or a decrease in the Schottky barrier allowing charge carriers to pass through more easily.

Purpose of Hall measurements

Mobility is a description of how strongly an electric field influences the motion of a charge carrier [16]. It is a function of the charge, q, the mean free time between collisions, τ_c, and the effective mass of the charge carrier, m_n. Mobility is defined as

$$\mu \equiv q\tau_c / m_n \quad [16]. \tag{3}$$

There are two factors that affect charge carrier mobility: lattice scattering and ionized impurity scattering. Lattice scattering is the result of the temperature-dependent motion of the lattice and dominates at high temperatures when the lattice constituents have high kinetic energy. Impurity scattering is the result of Coulombic interactions between ionized impurities and the charge carriers passing through the lattice. Impurity scattering dominates at low temperatures when the lattice constituents and charge carriers have less kinetic energy, so that the charge carriers spend more time in the vicinities of the impurities and are less affected by lattice vibrations.

Mobility as well as sheet charge carrier density can be determined using the Van der Pauw technique. The Van der Pauw technique has two parts: a sheet resistance measurement and a Hall voltage measurement. The Hall voltage measurement gives the

sheet carrier concentration, which is combined with the sheet resistance to calculate mobility as

$$\mu = 1/qn_sR_s \quad [22]. \tag{4}$$

To determine the sheet resistance, two characteristic resistances must be calculated: R_A and R_B. R_A is calculated by applying a DC current through the sample from two contacts (1 and 2), while the voltage is measured from two other contacts (3 and 4) that are connected parallel to the current path between contacts 1 and 2 and applying Ohm's law (R = V/I) (see Figure 6). R_B is calculated by applying a current through the sample from contact 2 to contact 3 while measuring the voltage from contact 1 to contact 4 (Figure 6).

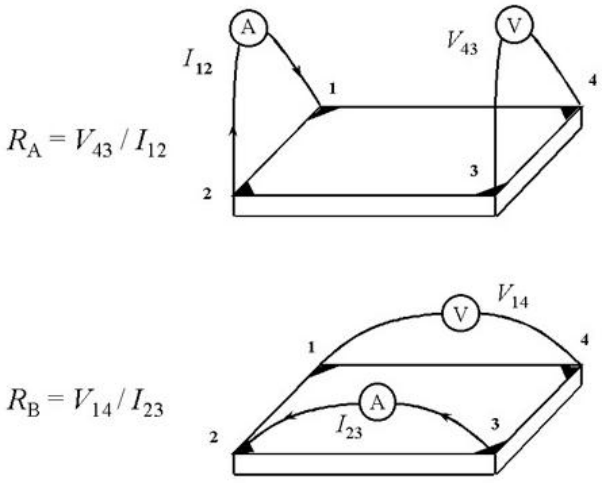

Figure 6. This demonstrates how to determine the characteristic resistances of a semiconductor sample using the Van der Pauw technique. Image used without permission from [22].

For improved accuracy, the current can be reversed for each measurement and the voltage re-measured and averaged with the first measurement. Finally, R_A and R_B are applied to the Van der Pauw equation

$$e^{-\pi RA/RS} + e^{-\pi RB/RS} = 1, \quad (5)$$

which is then solved numerically for R_S, the sheet resistance [22].

The Hall voltage is determined by placing the sample into a magnetic field perpendicular to the plane of the sample, applying a DC current diagonally across the sample, and measuring the voltage across the other diagonal connection as shown in Figure 7.

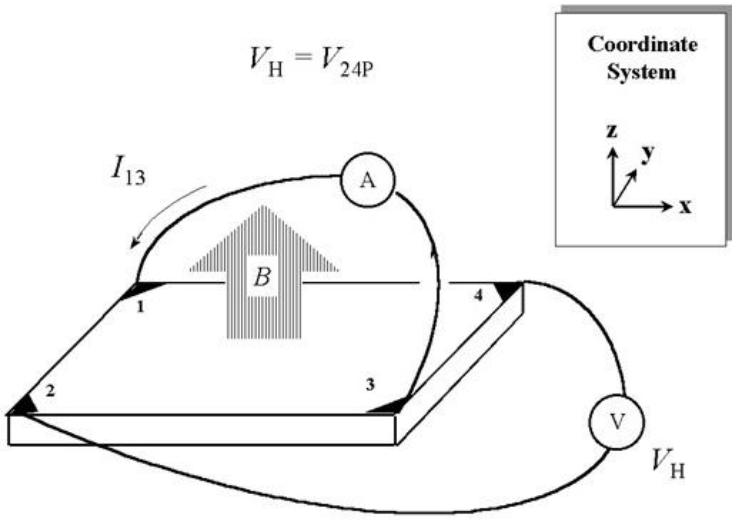

Figure 7. Determining the Hall voltage (V_H) involves applying a current diagonally across the sample and measuring the voltage at the other two points. Image used without permission from [22].

Again, the accuracy can be improved by reversing the current and repeating the measurement, then applying the current across contacts 2 and 4 and repeating the voltage measurements. The magnetic field is reversed and the entire procedure is repeated in order remove any bias due to sample geometric inconsistencies. Taking the difference between each pair of voltages with the magnetic field in both directions (V_{13+} and V_{13-} for example) returns four Hall voltages the sum of which is used to calculate sheet carrier density according to

$$n_s = 8x10^8 IB / q(V_1 + V_2 + V_3 + V_4), \quad (6)$$

where I is the current in amperes, B is the magnetic field in gauss, and q is electronic charge in Coulombs [22]. (If the voltage sum is positive, then the sample is p-type, and the sheet carrier density is p_s.)

If the conducting layer thickness is known, the resistivity can be calculated by multiplying R_s by the thickness, and the bulk carrier density can be calculated by dividing n_s by the thickness. A Hall measurement worksheet can be found in the Appendix along with the corresponding experimental data for comparison.

Changes in mobility and carrier concentration as functions of fluence will aid in analysis of the traps that develop as a result of irradiation. For example, an increase in carrier concentration, while mobility remains constant, indicates trap formation and tunneling through the Schottky junction, while an increase in mobility, while carrier concentration remains constant, indicates traps forming and tunneling occurring in the AlGaN.

III. Experimental Procedure

A. Equipment and Planning

The irradiation experiments took place at the Sandia National Laboratories' Ion Beam Lab (IBL) using the 400 kV implanter beam line (Figure 8). The stated energy range of the beam line was 10 to 400 keV. To minimize any chemical changes caused by the irradiation in the device, nitrogen ions were used. Transport of Ions in Matter (TRIM) software was used to model transport of ions into the samples. The "collision events" charts, which used the modified Kinchin-Pease approximation of damage production, provided the method of determining the nitrogen ion energy. The modified Kinchin-Pease model assumes elastic collisions between hard spheres and considers electronic stopping, along with atomic interactions [23]. With a beam normal to the sample face, 10 keV was the optimal energy for the 200 Å passivation layer. However, the IBL had never used a nitrogen beam before, and they had had difficulty in keeping other ion beams from diverging at 10 keV. Consequently, an energy of 15 keV was used for the 200 Å, and the sample was rotated 45 degrees. The TRIM output is shown in Figure 9.

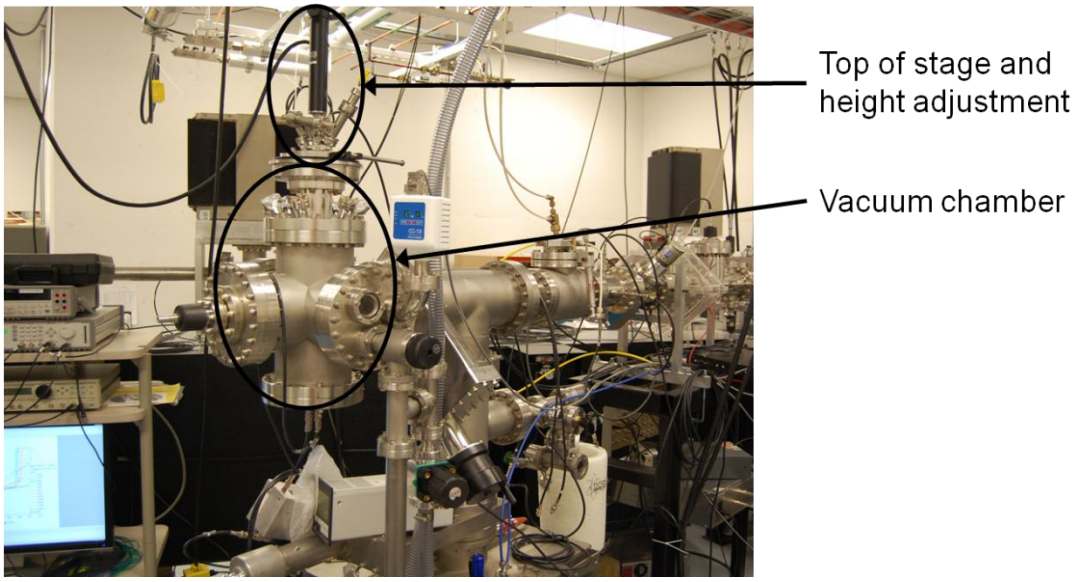

Figure 8. 400 kV implanter beam line at Sandia National Laboratories' Ion Beam Lab. The sample was loaded into the vacuum chamber at the top. The stage can be raised and lowered within the vacuum chamber.

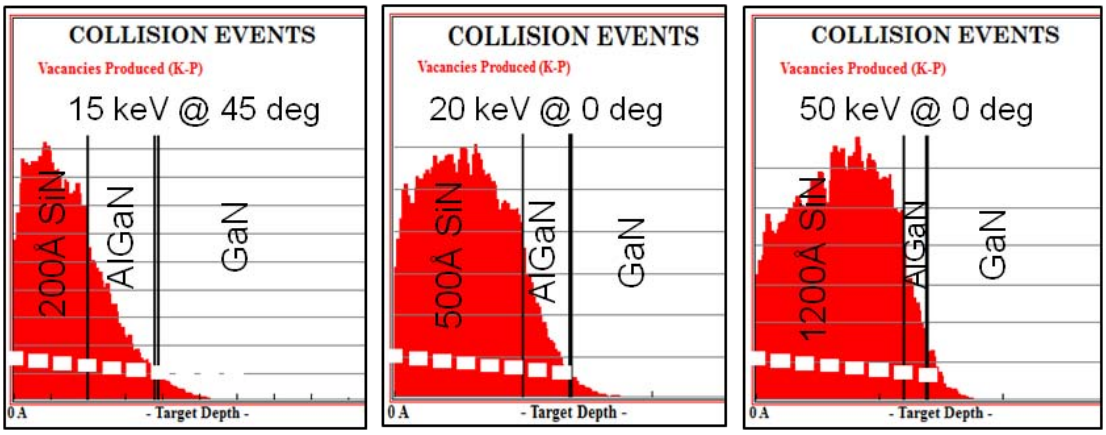

Figure 9. TRIM collision events charts for N+ irradiation of the three thicknesses of the Si_3N_4 passivation layer at energies designed to cause most of the damage in the Si_3N_4.

N^+ fluence levels were chosen to be equivalent to a fluence of 10^{16} cm^{-2} of 1 MeV electrons in order to be able to decouple ionization from displacement damage in future electron-irradiation research on other samples from this same wafer. Data from the TRIM models were used to calculate the nonionizing energy loss (NIEL) of the N^+ according to the procedure described by [24]. NIEL data was derived from the VACANCY.TXT file

from the TRIM simulations. The VACANCY.TXT gives information about vacancy formation in units of # vacancies/Å/ion. "The vacancy formation rate can be converted into NIEL using the modified Kinchin-Pease relationship between the number of atomic displacements…and a given quantity of nonionizing energy" according to

$$N_d = 0.8\frac{E_n}{2T_d}, \tag{7}$$

where N_d is the number of atomic displacements, E_n is the non-ionizing energy, and T_d is the threshold energy for atomic displacement [24]. Then the equations

$$F(T_0, Z, A) = 2\pi T_{\max}\frac{N_A}{A}\frac{r_0^2 Z^2(1-\beta^2)}{\beta^4} \text{ and} \tag{8}$$

$$NIEL = F(T_0, Z, A)\sum_{j=0}^{4}[a_j\int_{\theta_{\min}}^{180}\frac{(1-\cos(\theta+2\eta))^{(j-4)/2}}{1+\kappa_L * g(\varepsilon)}\sin^2(\theta/2)\sin(\theta)d\theta \tag{9}$$

were used to calculate the NIEL caused by the electrons [25]. Multiplying the maximum calculated value for NIEL in each Si_3N_4 layer by the ratio of the electron NIEL to the nitrogen NIEL determined what ion fluence was needed to achieve the equivalent of 10^{16} cm^{-2} 1 MeV electrons shown in

Table 2.

Table 2. Target fluences for the passivated samples. The unpassivated sample was irradiated to the same fluence as the 200 A sample.

Passivation layer thickness (Å)	Fluence (N^+/cm^{-2})
200	$1.8x10^{10}$
500	$2.0x10^{10}$
1200	$2.2x10^{10}$

B. Device Preparation

The AlGaN/GaN heterostructures used in this research were fabricated on a SiC-4HP substrate manufactured by Cree Inc. The 2 in. wafer consists of a 1000 Å AlN nucleation layer, a 17000 Å GaN buffer layer, a 10 Å AlN interlayer (any effects due to this interlayer are not within the scope of this research), and a 180Å AlGaN barrier layer. The epilayer supplier was IQE/Emcore. The layers were grown using metal oxide chemical vapor deposition (MOCVD) in August 2006.

The ohmic and gate contacts were fabricated by the Air Force Research Laboratory's (AFRL) Sensors Directorate, Devices and Sensing Branch (RYDD). Each ohmic contact consisted of a stack of titanium, aluminum, nickel, and gold (Ti/Al/Ni/Au). The gate contacts were 0.5 mm in diameter and consisted of 400 Å gold on 200 Å nickel. Once the wafers were metalized, they were cut into quarters for passivation. One quarter was left unpassivated. The other three quarters were passivated with 200 Å, 500 Å, and 1200 Å of Si_3N_4. Then all quarters were cut into 5 x 5 mm squares. An edge-on diagram is shown in Figure 10. Two samples from the unpassivated and 200 Å passivation thickness and three samples from the 500 Å and 1200 Å passivation thicknesses were chosen and cleaned using a 10-15 second acetone rinse followed by a 10-15 second isopropyl alcohol rinse. The samples were dried using nitrogen. Samples were labeled according to their passivation thickness and with the numeric -1, -2, or -3 added as they were taken from the wafer (0-1, 200-1, etc.). The samples were mounted on a circuit board backing and the contacts connected to tracings on the board. The gate contact was wire bonded and the ohmic contacts soldered using indium tin solder, which has very low electrical resistance. The final structure in the mount is as shown in Figure 11.

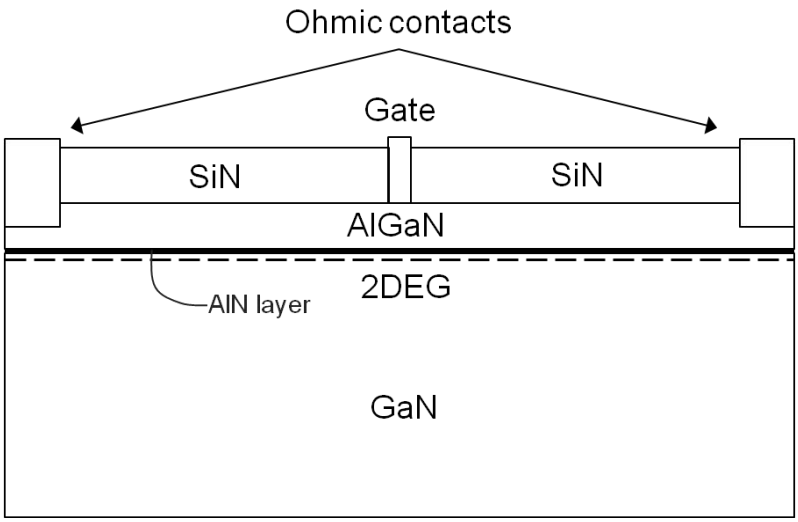

Figure 10. Edge-on diagram of passivated sample (not to scale)

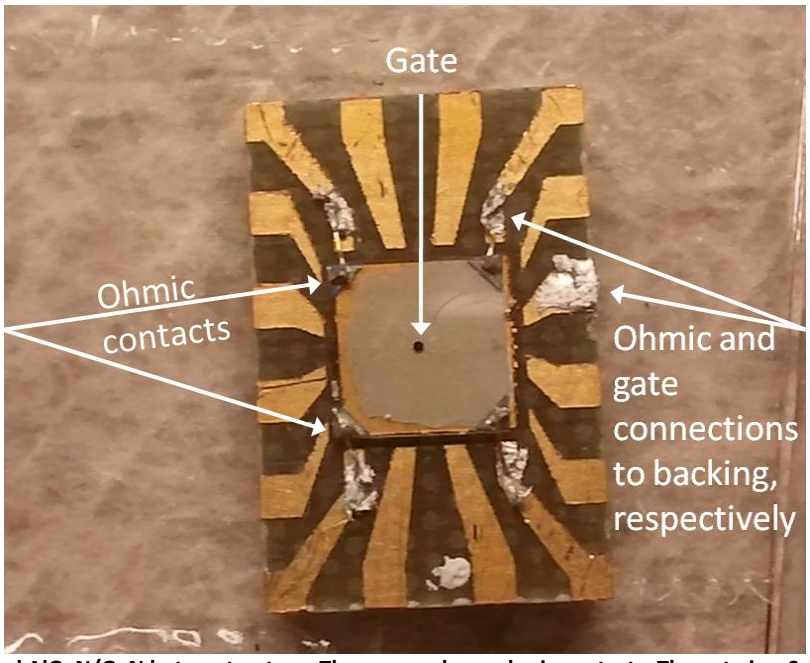

Figure 11. Mounted AlGaN/GaN heterostructure. The corners have ohmic contacts. The gate is a Schottky contact 0.5 mm in diameter. The contacts are connected to the circuit board backing via wire bonding for the gate and In-Sn solder for the ohmic contacts.

Pre-characterization Hall, C-V and I-V measurements were completed at AFIT and again at the IBL. The 0-1, 200-1, 500-1, and 1200-1 samples were kept as controls,

while 0-2, 200-2, 500-2, 500-3, and 1200-2 were irradiated. (Sample 1200-3 was not irradiated due to time constraints.)

Hall measurements were accomplished using an Ecopia HMS-3000 system. The samples were mounted on a spring probe mounting board with double-sided tape, and the probes were set on the gold strips on the backing to which the ohmic contacts had been connected. The Hall measurement input settings were 0.54 T magnetic field, 300 K temperature, and 0.54 mA current. The end of the mounting board was inserted into the lid of the system and the sample was inserted into the center column of the system as shown in Figure 12.

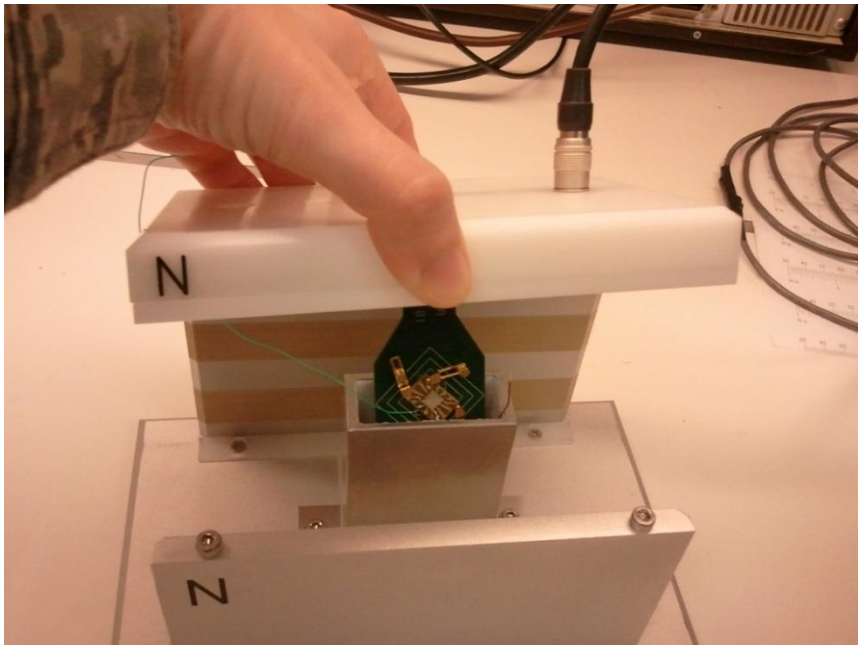

Figure 12. Sample on a spring probe mounting board for Hall measurements. The magnet pair slides in north-to-south, then south-to-north during the course of each measurement.

Due to the insulating nature of the silicon carbide substrate, C-V and I-V measurements were made by connecting the voltage source to the gate and reading the capacitance and current from one of the ohmic contacts on the corners as shown in Figure

13, rather than measuring vertically through the device. Capacitance was measured from inversion to accumulation at 1MHz on the Keithley 590 CV Analyzer. Using 1MHz "reflects only the charge variation in the depletion layer and the (rather small) movement of the inversion layer charge" [26].

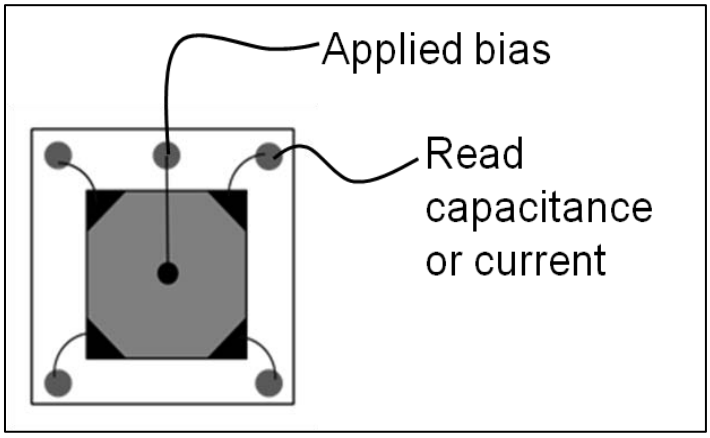

Figure 13. Wiring diagram for C-V and I-V measurements Leads from the gate and ohmic contacts were connected to circuit board backing. Wires for connecting the C-V and I-V meters (in turn) were then soldered to the corresponding points on the circuit board.

C. Experiment

It was possible to do multiple irradiations per sample as well as *in-situ* C-V measurements leading up to the desired fluences. The 400 kV implanter beam line was used to irradiate the samples. Samples were mounted onto a copper stage with double-sided tape as shown in Figure 14. The leads were connected to clips for *in-situ* C-V and I-V measurements. C-V measurements were made using a Keithley 590 C-V Analyzer. I-V measurements were made using a Keithley 2400 SourceMeter.

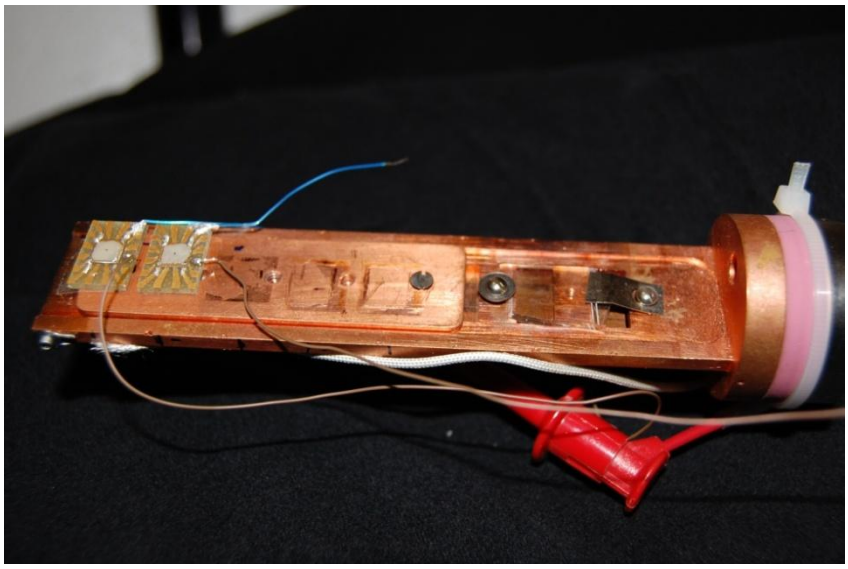

Figure 14. Sample 200-2 (far left) and 0-2 (second from left) on the stage for the 400kV implanter line at SNL's IBL. These two samples were mounted together since they would be using the same beam energy as well as to save time in loading, unloading, and pumping down the chamber. In this case, only the 200-2 sample was measured *in-situ*, while the 0-2 sample was measured after the samples were removed and after the Hall measurements before they were replaced in the chamber.

C-V measurements were initially coupled as a function of fluence. The initial irradiations were completed using 20 keV N^+ ions on sample 500-2.The beam area was 6 × 6 mm, completely overlapping the sample. The beam current was 2 nA, and each pulse length was 10 ms. Three irradiations of 10^8 20 keV N^+/cm^2 followed by *in-situ* C-V irradiation measurements resulted in no significant change in the C-V curve. Two additional irradiations and measurements were performed for a total fluence of 10^9 N^+/cm^2, again resulting in no significant change in C-V (see Figure 20).

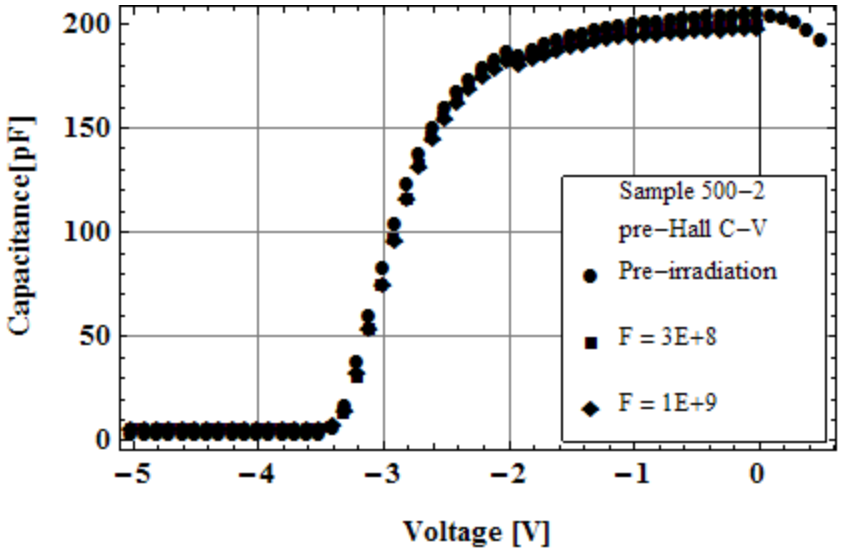

Figure 15. Post-irradiation pre-Hall C-V curves for sample 500-2. There was neglible change in C-V relationship after irradiation up to a fluence of 10^9 N^+/cm^2.

At this time, the sample was removed from the chamber for Hall measurements. A set of five Hall measurements was performed. Carrier mobility averaged the same as in pre-irradiation measurements; however, sheet carrier density decreased about 2.7%. Five and a half hours later, Hall and C-V were measured again to determine post-irradiation time-dependent effects. The average mobility had decreased ~2.5%, while average carrier density decreased ~1.2%from pre-irradiation carrier density, as shown in Figure 16 and Figure 17. The AlGaN capacitance also changed significantly during the time it took to make the Hall measurements as shown in the very low, stretched-out C-V curves in Figure 18. Capacitance roll-off in accumulation was also observed (Figure 18). Roll-off has been attributed to both series resistance [27] and gate leakage currents [28], [21].

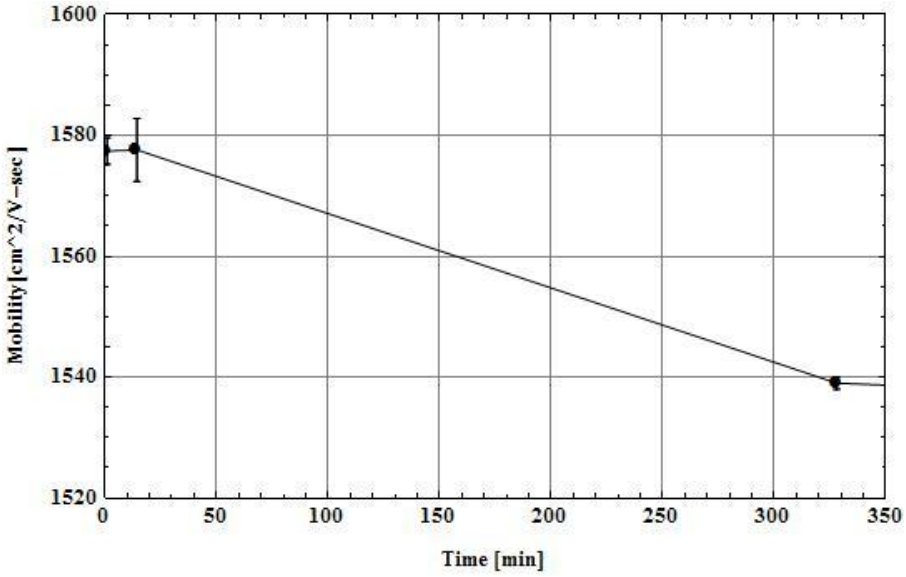

Figure 16. Mobility measurements for sample 500-2 before irradiation, shortly after irradiation and after 5.5 hours

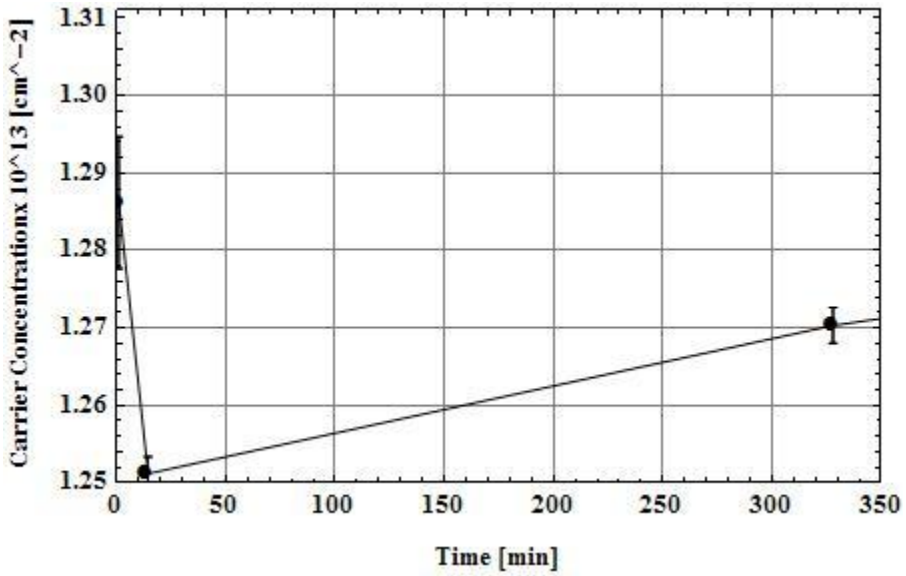

Figure 17. Carrier concentration measurements for sample 500-2 before irradiation, shortly after irradiation and after 5.5 hours

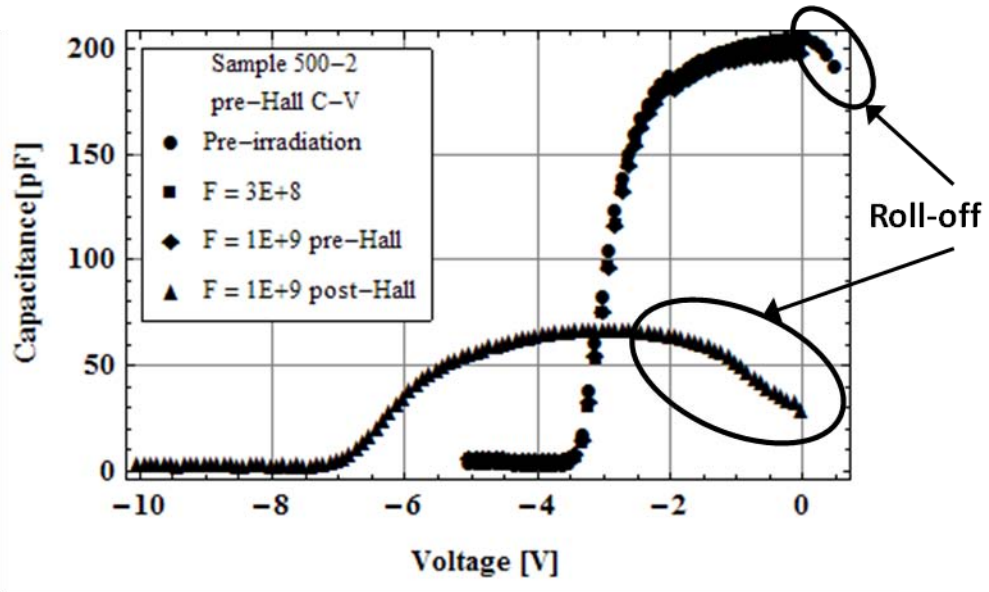

Figure 18. C-V curve of sample 500-2 after irradiation and Hall measurements. The AlGaN capacitance decreased by 130 pF, and V_{th} shifted about 3.5 V in the negative direction. Roll-off occurs in accumulation as a result of leakage through thin gates and channel, contact, or other series resistances [27], [28], [21].

The second sample irradiated was the 500-3 sample. C-V, and Hall measurements were coupled as a function of fluence. Since the pump-down time was approximately 45 min, the irradiation and measurement process took three hours for each of the three beam experiments.

The 500-3 sample was irradiated for 100 ms at a time, with a beam current of 2 nA, three times for a total fluence of 2×10^{10} N^{+}/cm^{2}. The beam energy was 20 keV. C-V as well as I-V measurements were completed immediately after each irradiation while the sample was still under vacuum. The chamber was then vented, the sample removed and carrier concentration and mobility were measured using the Hall system. The sample was returned to the chamber, C-V and I-V were measured again, and then the chamber was pumped down for the next irradiation.

The 1200-2 sample was irradiated with 50 keV nitrogen ions. The target fluence was 2.2×10^{10} N^{+}/cm^{2}. Beam current was about 2 nA. The wire soldered to the gate lead

on the sample backing broke and had to be re-soldered. The sample was then mounted on the stage and placed in the chamber. The capacitance was then measured and did not have a characteristic C-V shape. Rather the top sloped steeply down to the left (negative) almost linearly with a slight knee around -3 V (see Figure 22). Due to time constraints the procedure was continued using this sample "as-is," After irradiating to 7.29×10^{9} N^{+}/cm^{2}, C-V and I-V were measured with the sample still under vacuum. Then the chamber was vented, the samples removed, and carrier concentration and mobility were measured. The sample was replaced on the stage and into the chamber. Another set of C-V and I-V were measured again prior to pump-down.

For the second irradiation, beam current was 2.37 nA, requiring a pulse time of 180 ms for a fluence of 7.4×10^{9} N^{+}/cm^{2} (total fluence 1.47×10^{10} N^{+}/cm^{2}). Again C-V and I-V were measured immediately after the irradiation, followed by the Hall measurements. The C-V and I-V curves overlapped the previous ones; however, the mobility increased after this irradiation, while carrier concentration decreased by only 1% from pre-irradiation measurements. The procedure was repeated for the third irradiation (beam current = 2.1 nA, t = 200 ms, F = 7.29×10^{9} N^{+}/cm^{2}). Because the Hall data did not present a consistent increase or decrease in either mobility or carrier concentration, the sample was irradiated a fourth time. The fourth irradiation was at a beam current of 1.7 nA for 250 ms providing a fluence of 7.38×10^{9} N^{+}/cm^{2} and a total fluence of 2.94×10^{10} N^{+}/cm^{2}. AlGaN capacitance continued to decrease. Hall measurements resulted in a decrease in both mobility and carrier concentration.

The 0-2 and 200-2 samples were irradiated simultaneously (see Figure 14) to reduce time at the IBL. They were set at an angle of 45 degrees to surface normal (see Figure 19) and irradiated with 15 keV nitrogen ions. This was done in order to get damage events equivalent to 10 keV nitrogen ions at 0 degrees. It was not initially believed that the 400 kV implanter could get a nitrogen beam with an energy as low as 10 keV; however, experience with the 15 keV beam indicated that a 10 keV nitrogen beam would be possible.

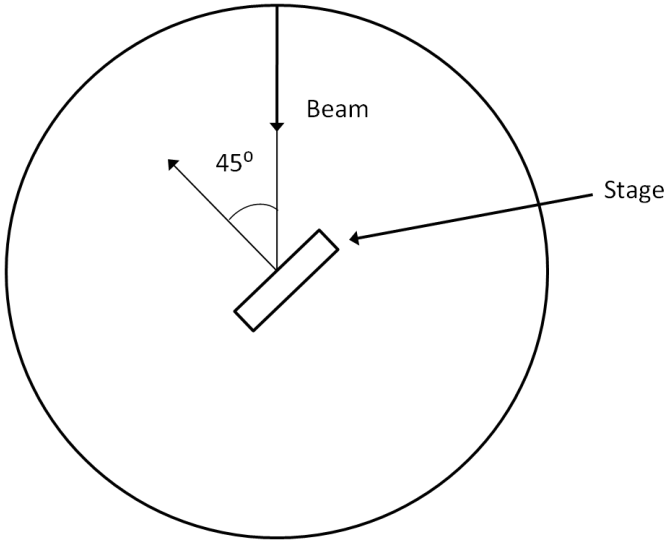

Figure 19. Diagram of a top-down view of the evacuation chamber with the stage rotated 45 degrees with respect to beam direction.

Sample 200-2 was connected and measured *in-situ* while sample 0-2 was measured out of the chamber after each irradiation. The total target fluence for these samples was 1.8×10^{10} N^+/cm^2. The beam current for the first two irradiation was 2.15 nA and was pulsed for 160 ms for a fluence of 5.97×10^9 N^+/cm^2 for each irradiation. The beam current for the third irradiation was 2.0 nA and was pulsed for 165 ms for a fluence of 6.04×10^9 N^+/cm^2. Total fluence achieved was 1.84×10^{10} N^+/cm^2.

Immediately after each irradiation, C-V and I-V were measured under vacuum on sample 200-2. The chamber was then vented, the samples removed, and sample 0-2 was connected for C-V and I-V measurements. Finally, the samples were removed one at a time from the stage for Hall measurements.

Table 3. Fluence per irradiation for each sample

Sample	Fluence per irradiation (N+/cm^2)				Total Fluence
	1	2	3	4	
500-2	1.0E+08	1.0E+08	1.0E+08	6E+08	1E+09
500-3	6.7E+09	6.7E+09	6.7E+09		2.00E+10
1200-2	7.29E+09	7.40E+09	7.29E+09	7.38E+09	2.94E+10
0-2 200-2	6.0E+09	6.0E+09	6.0E+09		1.84E+10

IV. Results and Analysis

A. Results of C-V Measurements

All samples showed evidence of roll-off in accumulation, particularly the passivated samples. Roll-off of capacitance in accumulation indicates the presence of added series resistance [27]. The unpassivated sample (0-2) retained its peak between 0 V and 0.5 V, whereas the passivated samples experienced a negative shift in peak capacitance. All samples experienced a decrease in capacitance after irradiation coupled with exposure to the Hall magnetic field.

Sample 500-2

No significant change was noted in the C-V curves after the first three irradiations totaling a fluence of 10^9 N^+/cm^2, so one more irradiation was made. Again there was no significant change in C-V. A fifth irradiation for a total fluence of between 8×10^8 and 10^9 $N+/cm^2$ was made with the same results. It was not until after Hall measurements were made that the C-V response curve changed. AlGaN capacitance decreased significantly, almost 75%, shifted toward negative voltage, and stretched out, as can be seen in Figure 20. All five samples showed similar behavior.

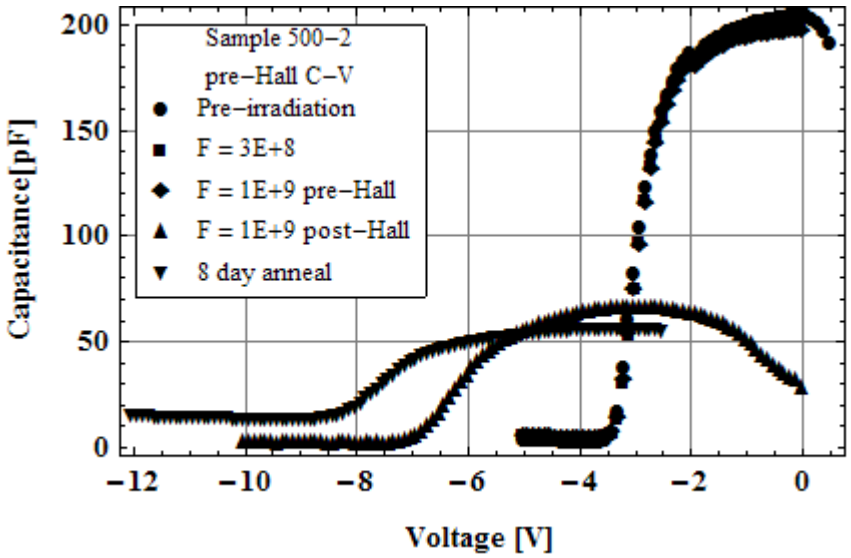

Figure 20. C-V measurements for sample 500-2. There was little if any change in C-V data immediately after each irradiation; however significant change can be seen for C-V measurements taken after Hall measurements.

Sample 500-3

Immediately after the first irradiation, the AlGaN capacitance increased by 50%, to ~100 pF. However, C-V measurements taken after the first set of Hall measurements had a 54% decrease in AlGaN capacitance compared to pre-irradiation, a -2 V shift in V_{th}, and stretch-out in depletion. Measurements after the second and third irradiations were more consistent but continued to demonstrate a decrease in AlGaN capacitance, a negative shift in V_{th}, and stretch-out (see Figure 21).

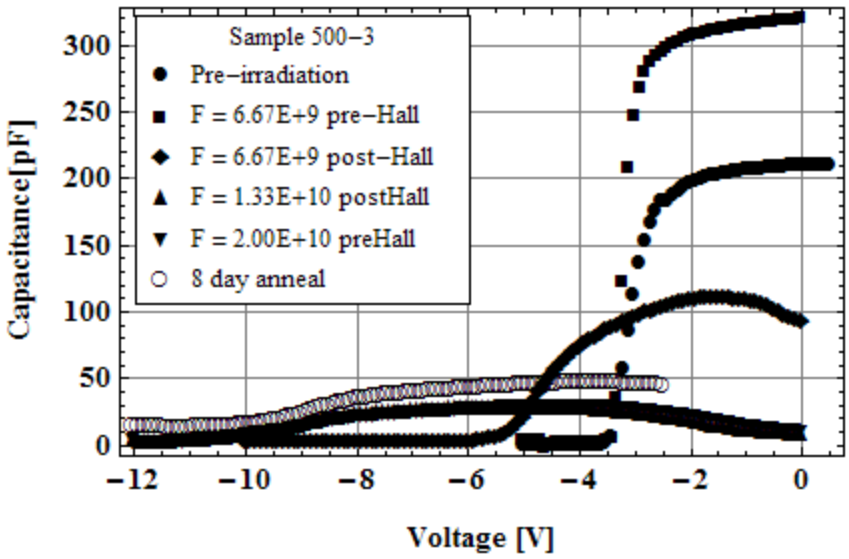

Figure 21. C-V curves for sample 500-3. The AlGaN capacitance initially increased by 50% after irradiation but then decrease to 50% of the pre-irradiation capacitance after the Hall measurements were done. Continued irradiation and Hall measurements led to a continued decrease in AlGaN capacitance.

Sample 1200-2

One of the wires on the 1200-2 sample broke shortly before irradiation and needed repair. A new pre-characterization C-V curve was measured in the chamber and had an uncharacteristic shape. In the interest of time, the procedure was continued with the sample "as is." The AlGaN capacitance dropped from 194.8 pF at 0 V to 58.76 pF at 0.7 V. There was also a slight shift in the negative direction; however, there was no way to identify stretch-out due to the significant slope already in existence (See Figure 22). Due to the poor shape of the 1200-2 curve, not much more information can be elicited from the data.

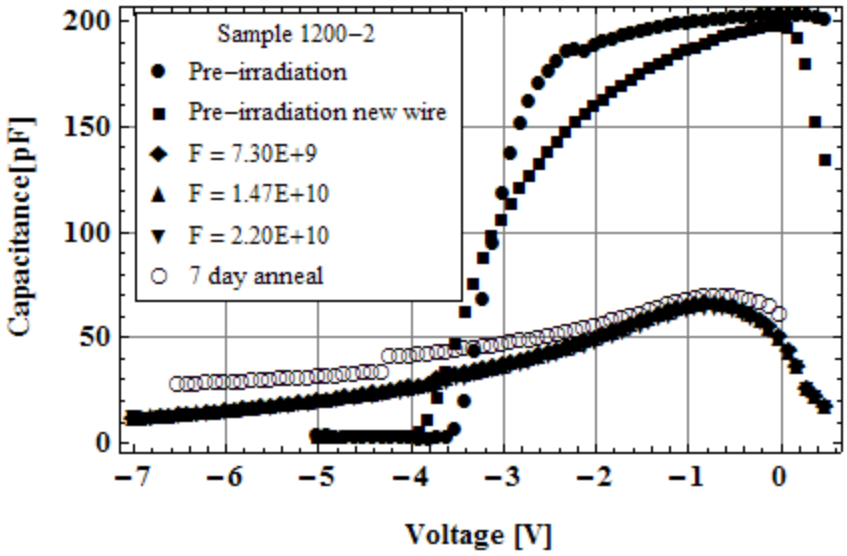

Figure 22. C-V curves for sample 1200-2. Due to a poor connection in a replaced wire, this data is only of qualitative use.

Sample 0-2

AlGaN capacitance for sample 0-2 decreased over the first two irradiations after the Hall measurements. V_{th} shifted ~ -1 V after the Hall measurements after the second irradiation (F = 1.20×10^{10} N^{+}/cm^{2}). Capacitance recovered somewhat after the third irradiation before the Hall measurements but could not be measured after the Hall measurements because the gate wire had broken.

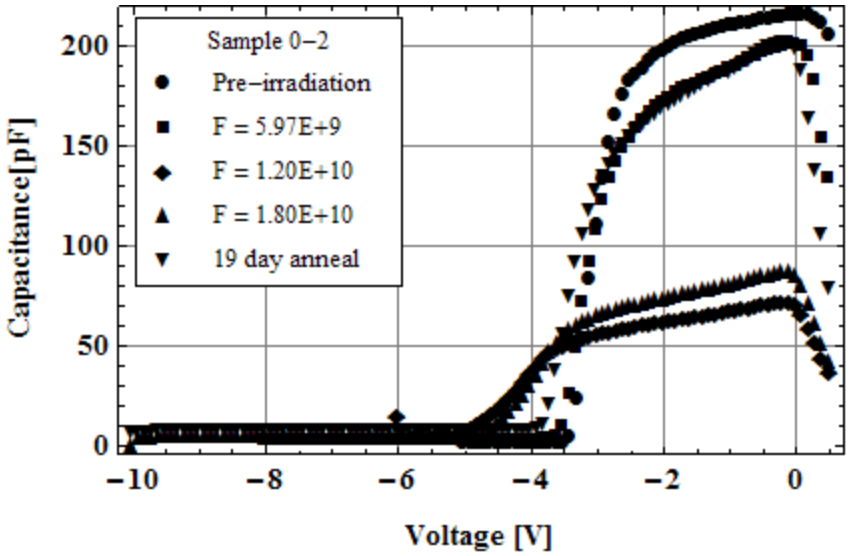

Figure 23. C-V curves for sample 0-2 measured post-Hall measurements except for F = 1.80x10^{10} N+/cm^{-2} which was measured before Hall measurements. The gate wire became disconnected from the gate during the Hall measurements, so post-Hall C-V could not be measured until after annealing.

In all five samples irradiated, the AlGaN capacitance usually decreased as a function of fluence and possibly time. In all the samples, other than 1200-2, V_{th} shifted by more than -3 V. Additionally, the C-V measurements of all the samples eventually showed stretch-out in depletion. Only sample 0-2 showed recovery in AlGaN capacitance and ΔV_{th} over time—after 19 days, capacitance had recovered to the same level as after the first irradiation of F = 5.97×10^9 N$^+$/cm^2, and there was only a slight (-0.3V) shift in V_{th} (Figure 23).

Changes in Capacitance

Capacitance in inversion increased slightly for the passivated samples, most noticeably after annealing for about one week. This could indicate a change in effective donor doping levels in the GaN [19] after irradiation except that, as shown in the TRIM charts in Figure 9, very little of the irradiation was expected to penetrate that far. The shifts are on the order of 10 pF, but it could also be due to the damage in the Si_3N_4.

AlGaN capacitance in each irradiated sample decreased by more than 50% by the last irradiation of each sample. AlGaN capacitance before irradiation measured ~200 pF for all samples. After irradiation, AlGaN capacitance measured between 50 and 100 pF for all but sample 500-3, which peaked around 30 pF. Using PSpice to model an equivalent circuit across the Schottky junction and AlGaN to the AlGaN/GaN interface (Figure 24) provided insight into what may be happening as a result of the irradiation. The variable (V1) and DC (V4) voltages represent the input from the C-V meter. The diode, D6, represents the Schottky junction at the gate/AlGaN interface. A negative DC voltage represents forward bias, and a positive voltage represents reverse bias. The resistance R2 represents the resistance within the AlGaN, and the diode D5 represents the AlGaN/GaN interface. Current was measured for several values of R at both +5 and -5 V. Capacitance was calculated as

$$C = I / (2\pi f V_1). \tag{10}$$

In reverse bias, the capacitance changed about half an order of magnitude, while in forward bias, the capacitance changed about 1.5 orders of magnitude as shown in Figure 25.

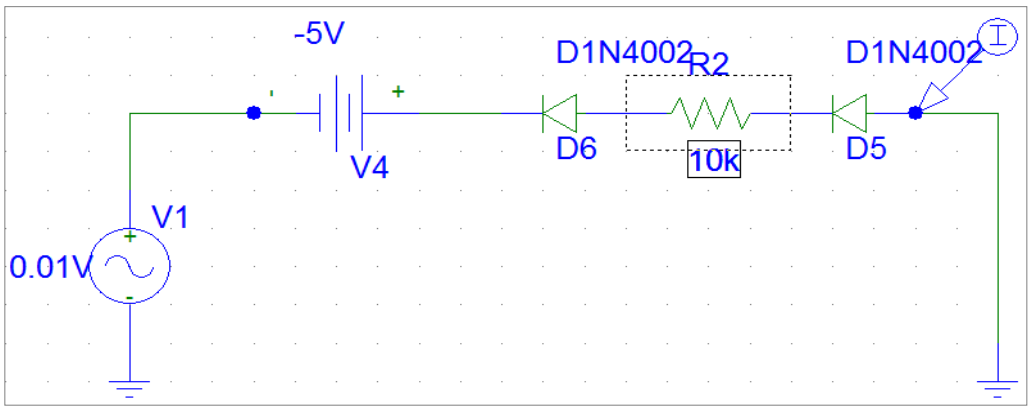

Figure 24. PSpice was used to model the Schottky junction (D6) ,AlGaN (R2) and AlGaN/GaN interface (D5). Increasing the value of the resistance decreased the current which is directly proportional to capacitance.

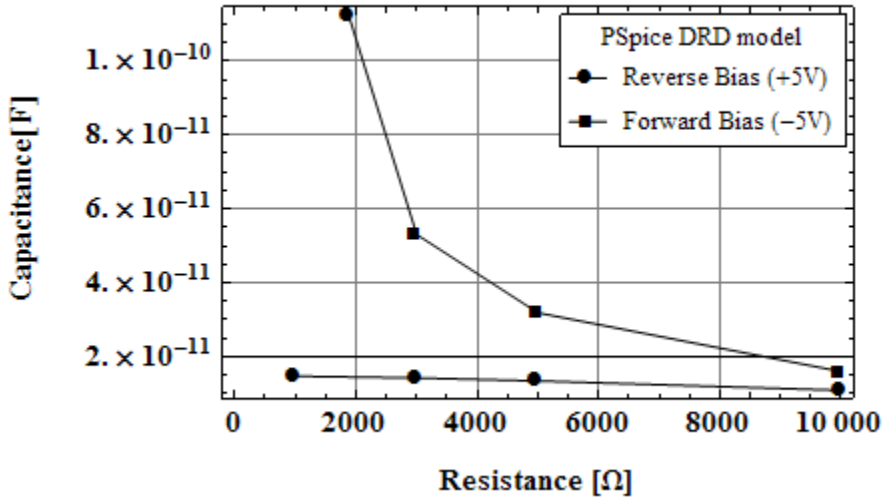

Figure 25. Capacitance vs. Resistance results from the PSpice model. In forward bias (-5 V) the capacitance decreases quickly as the series resistance increases.

Measurement of ΔV_{th}

The shift in V_{th} is attributed to electron-hole pairs being generated by the radiation and the holes getting trapped along the interface. As described in [19], this additional positive charge at the interface attracts more electrons to the 2DEG, which then requires a more negative gate voltage to deplete the gate. Interestingly, these shifts did not happen

until after the Hall measurements were done. This indicates that the electron hole pairs caused by the irradiation did not recombine. Rather the intrinsic field in the AlGaN moved the electrons elsewhere in the devices, Possibly there were trapped in the Si_3N_4 until they were swept out by the current applied during the Hall measurements.

Table 4 shows ΔV_{th} for each sample on the day of irradiation as well as upon return to AFIT. Sample 0-2 had to await repair before it could be measured post-trip and had nearly recovered to its pre-irradiation level. Figure 26 shows the nearly linear relationship between ΔV_{th} and passivation thickness both the day of irradiation and after annealing.

Table 4. Threshold voltage shifts in irradiated samples. ΔV_{th} is the total shift on the day of irradiation. ΔV_{th} final represents data taken upon return to AFIT. The gate wire on sample 0-2 broke during the last Hall measurement, so post-trip C-V measurement had to wait until the sample could be repaired.

Sample	ΔV_{th}	ΔV_{th} final	
0-2	-1.298	-0.404	19 days post-irradiation
200-2	-4.298	-3.704	7 days post-irradiation
500-2	-4.883	-5.100	9 days post-irradiation
500-3	-7.699	-6.599	9days post-irradiation
1200-2	insufficient data		

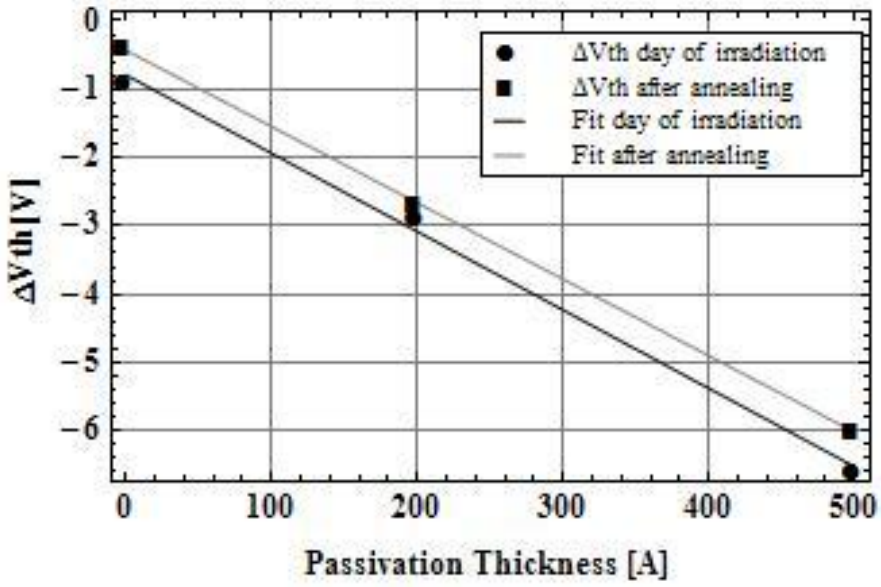

Figure 26. Change in threshold voltage in samples undergoing equivalent radiation: 0-2, 200-2, and 500-3. After irradiation and after annealing. The threshold volgtage shift in the unpassivated sample followed the linear trend despite the long anneal time (19 days for 0-2, 7 and 9 days for 200-2 and the 500s respectively.

Determination of C-V Stretch-Out

The estimated values for ΔN_{it} are shown in Figure 27. In the unpassivated sample, ΔN_{it} increases up until the post-Hall measurement after the second irradiation (1.20×10^{10} N^{+}/cm^{2}) and then decreases. It may have increased more after the third irradiation (1.80×10^{10} N^{+}/cm^{2}), but the gate wire broke and C-V could not be measured. By 19 days post-irradiation, the C-V had the same amount of stretch out as pre-irradiation indicating the interface trap concentration had returned to its pre-irradiation level.

In the passivated samples, ΔN_{it} increases with radiation and exposure to the Hall magnetic field after each of the first two irradiations. However, ΔN_{it} decreased in sample 200-2 after the last Hall measurement, and in sample 500-3, the capacitance has decreased to such an extent that ΔV_{it} is a very rough estimate and overlaps the pre-Hall value after the third irradiation.

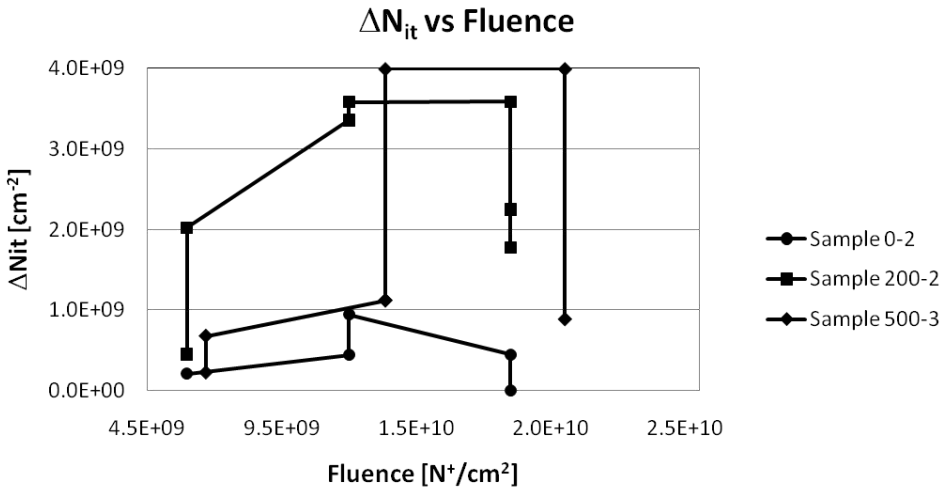

Figure 27. ΔN_{it} vs. fluence for samples 0-2, 200-2, 500-3. The vertical lines indicate measurements made before and after Hall measurements after each irradiation chronologically along the line. The last point of each data set represents ΔN_{it} after annealing. In the case of 500-3, there was no change after the Hall measurement after the third irradiation, so the pre-Hall and post-Hall data points overlap. In the case of 0-2, no post-Hall measurement could be made due to a broken gate lead.

Week-long post-irradiation annealing for each passivation thickness resulted in somewhat different responses in C-V measurements. All samples had an increase in capacitance in inversion, but the AlGaN capacitance in accumulation varied. Sample 200-2 had the same curve as it did immediately after irradiation. In sample 500-2 capacitance in the accumulation region was slightly lower than immediately post-irradiation. In sample 500-3 capacitance in the accumulation region was higher than immediately post-irradiation. The very large decrease in AlGaN capacitance for all samples over the course of irradiation and measurement and the significant leakiness of the samples after irradiation indicates significant displacement damage and trap formation enabling tunneling through the interface and AlGaN.

B. Results of I-V

In I-V measurements, the unpassivated sample (0-2) behaved differently from the passivated samples. The forward bias current decreased after irradiation and Hall measurements (Figure 28). In the passivated samples reverse-bias current increased (in the negative direction) and became nearly linear (Figure 29, Figure 30, Figure 31). Additionally, the current the current in the forward bias region between 0 V and 1 V increased slightly such that the slope of the curve through 0 V increased, indicating a decrease in resistance through the Schottky junction. Samples 0-2 and 500-2 experienced additional shifting after annealing. In the case of sample 0-2, the forward bias current returned to pre-irradiation levels. In the case of sample 500-2, the forward bias current decreased while the reverse bias current increased.

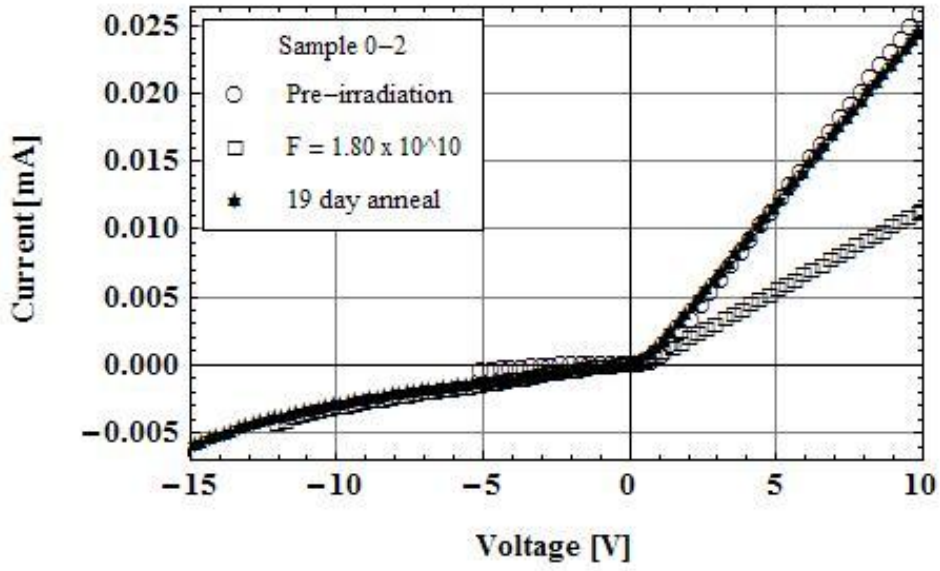

Figure 28. I-V curve for sample 0-2 (unpassivated). The reverse-bias current changes only slightly while the forward-bias current decreases more than 50% after irradiation and exposure to a 0.54 T magnetic field.

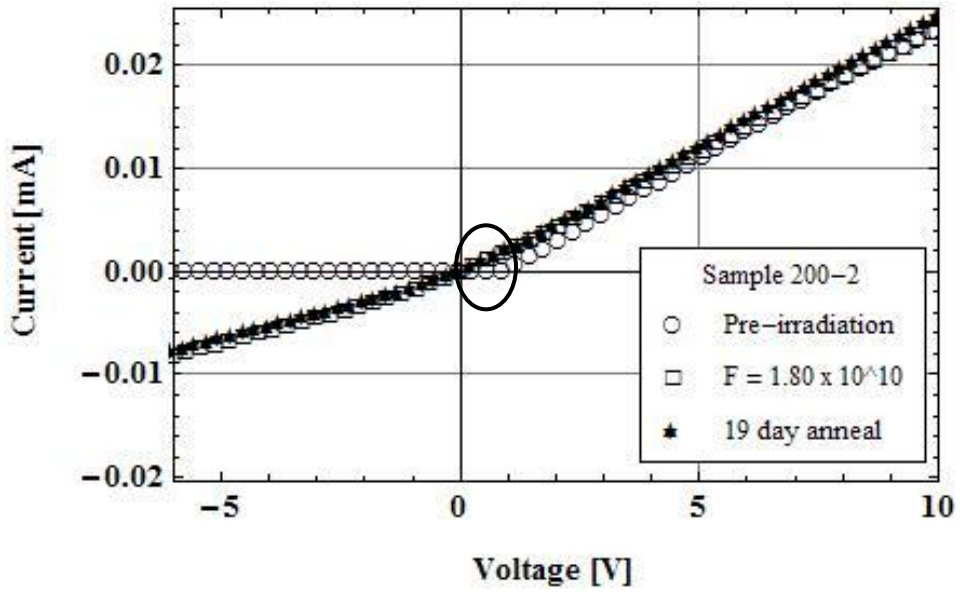

Figure 29. I-V curve for sample 200-2. The reverse bias current shifts about five times more than in the unpassivated sample, whereas the forward bias current increases slightly and mostly at 0 - 1 V where the Schottky barrier has the most effect.

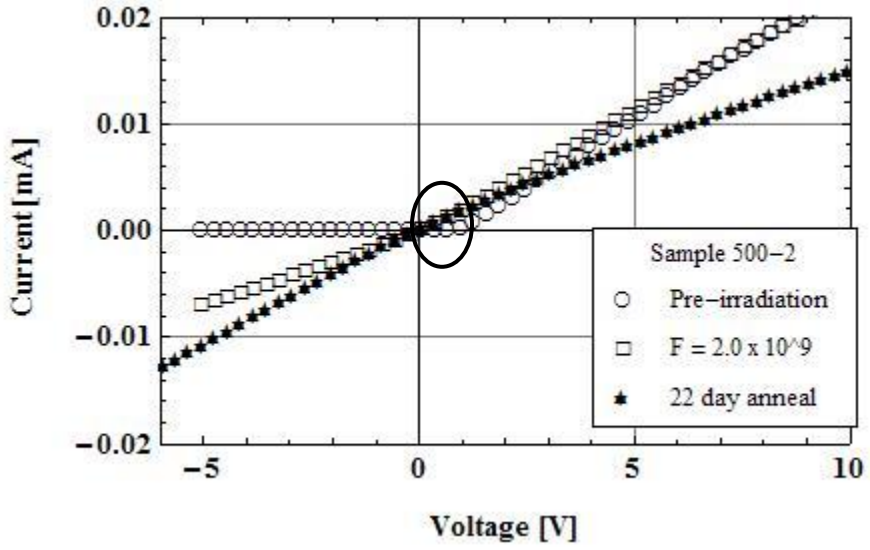

Figure 30. I-V curves for sample 500-2. This sample was exposed to a lower fluence than the other samples. Before annealing, the reverse bias current shifted in the negative direction on the same order as the sample passivated with 200 Å Si_3N_4. Interestingly, the current shifts in both forward and reverse bias *after* annealing. Unfortunately, there was insufficient data for the 500-3 sample to corroborate this effect.

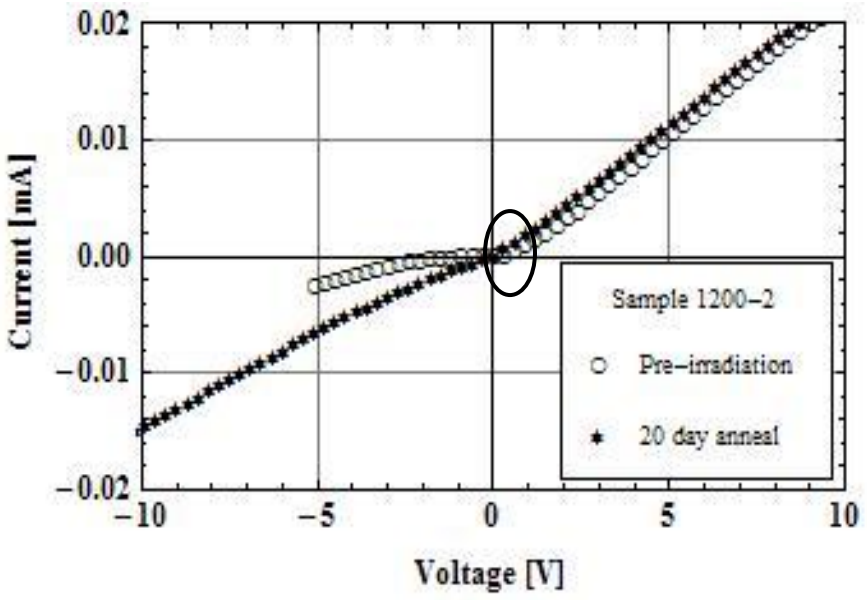

Figure 31. Pre-irradiation and post-anneal I-V curves for sample 1200-2. The reverse bias shift was less than that for 200-2 and 500-2 but greater than that for the unpassivated sample. The forward bias current after irradiation and annealing showed the same characteristics as the sample passivated with 200Å Si_3N_4.

An attempt was made to characterize the ideality factor as described in [16] for sample 500-2. A semi log I-V plot in the region of interest is shown in Figure 32. The slope is an indicator of the ideality factor. Neither of the lines has a slope near 1 or 2, which indicate a reduction in diffusion current due to an increase in series resistance (R_s). Series resistance can be calculated as

$$R_s = \frac{G_{ma}}{G_{ma}^2 + \omega^2 C_{ma}^2}, \tag{11}$$

where C_{ma} is the capacitance measured in strong accumulation, G_{ma} is the equivalent parallel conductance at accumulation, and ω is 2π times the measurement frequency [29]. Figure 33 shows calculated R_s before and after irradiation and after annealing as a function of passivation thickness. Prior to irradiation R_s was between 350 and 387 Ω. After irradiation, R_s nearly doubled, and R_s for the passivated samples persisted

near the post-irradiation values while it decreased nearly to its pre-irradiation value for the unpassivated sample (0-2). This increase in series resistance contributes to the decrease in the AlGaN capacitance after irradiation.

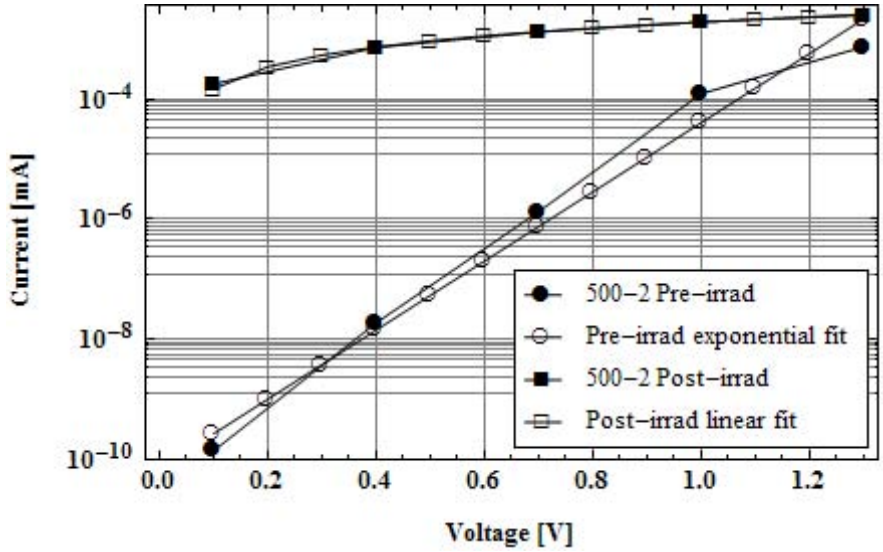

Figure 32. Semi log plot of current vs. voltage for sample 500-2. The ideality factor is indicated by the slopes of the lines. The current as a function of voltage develops a linear response through the Schottky junction after irradiation as opposed the the exponential response it has before irradiation.

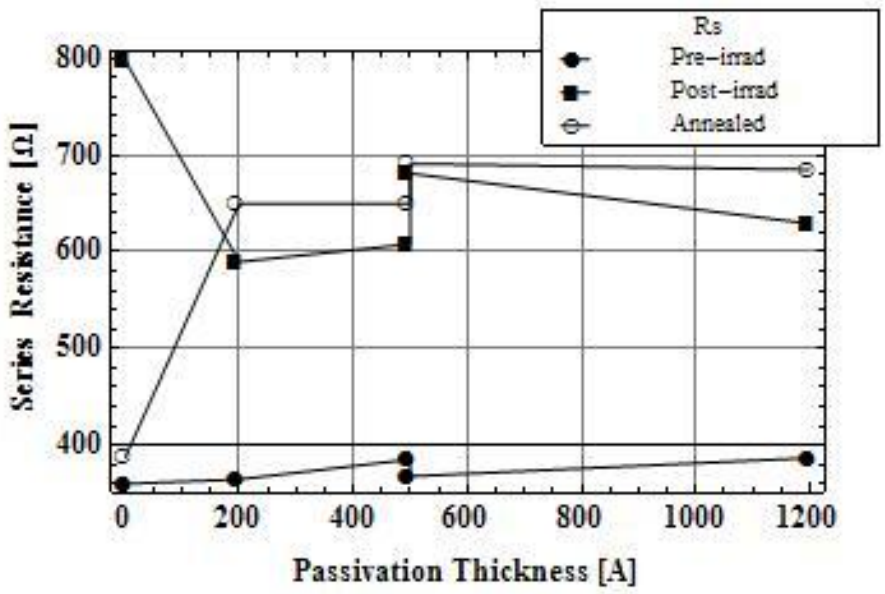

Figure 33. Series resistance (R_s) as a function of passivation thickness for samples 0-2, 200-2, 500-2, 500-3, and 1200-2 in order. R_s nearly doubles after irradiation and persists for the passivated samples, while R_s for the unpassivated sample (0-2) returns to near pre-irradiation level after a 19 day anneal.

C. Hall mobility and carrier concentration

Prior to irradiation, mobility and carrier concentration were measured in all samples. Figure 34 and Figure 35 show mobility and carrier concentration for each of the two unpassivated and 200 Å passivated samples and the three 500 Å and 1200 Å passivated samples. (The mobility of two of the 1200 Å samples was the same, around 1485 cm^2/V-sec.) Figure 36 and Figure 37 show the average post-irradiation values for mobility and carrier concentration as a function of fluence for the four samples that were irradiated with equivalent fluences of nitrogen ions (samples 0-2, 200-2, 500-3, and 1200-2). An increase in carrier concentration while mobility remains constant indicates traps forming and tunneling occurring in the Schottky junction, while the reverse effect indicates traps forming and tunneling occurring in the AlGaN.

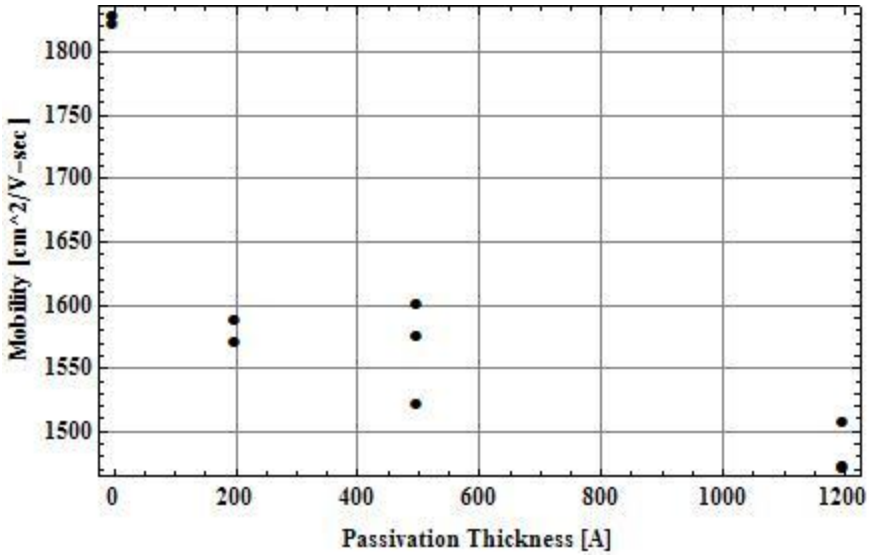

Figure 34. Carrier mobility as a function of passivation thickness in the AlGaN/GaN samples prior to irradiation. There were three 1200 Å samples, two of which had the same mobility (about 1485 cm^2/V-sec). Average mobility is at least 14% lower in these passivated samples than in the unpassivated samples.

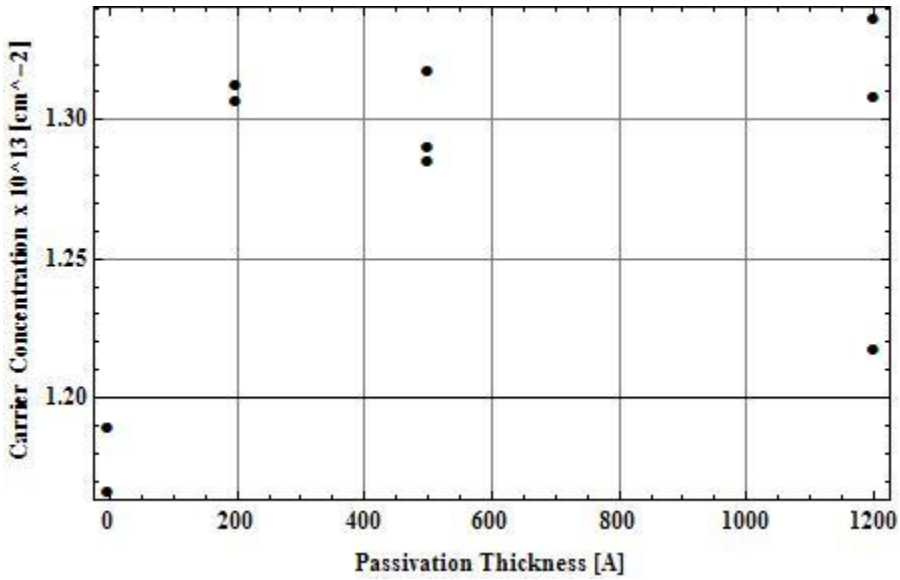

Figure 35. Carrier concentration as a function of passivation thickness in the AlGaN/GaN samples prior to irradiation. Average carrier concentration is highest (~11%) in the samples passivated with 200 Å Si_3N_4 and lowest in the unpassivated samples.

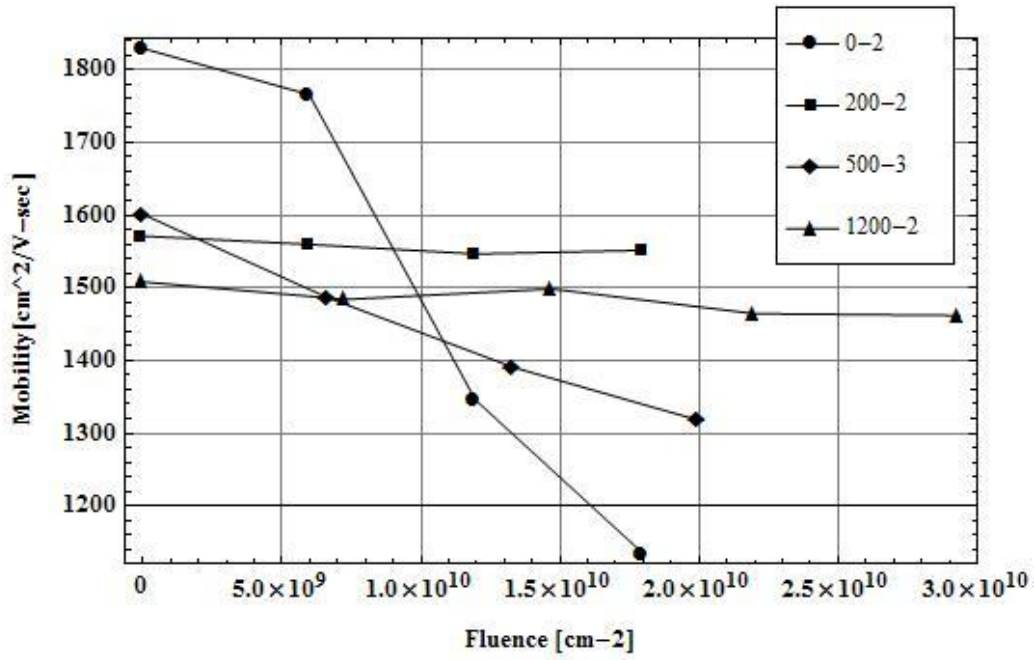

Figure 36. Carrier mobility as a function of fluence for the four samples that received equivalent fluences of nitrogen ions. Four data points were insufficient to determine if there was a trend in the change in mobility after each irradiation; therefore, there is a fifth data point for sample 1200-2.

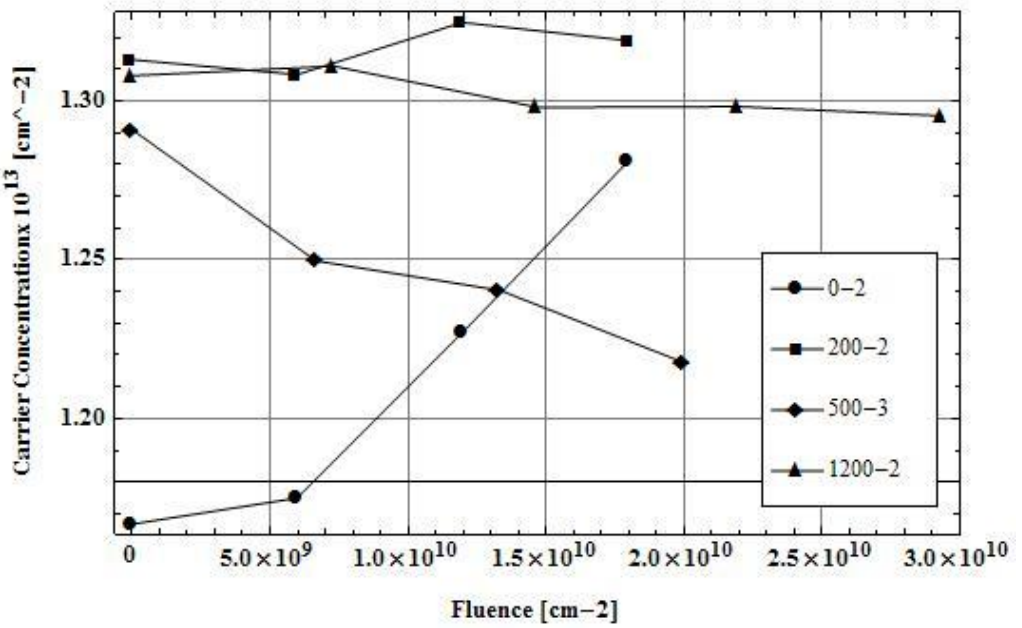

Figure 37. Carrier concentration as a function of fluence for the four samples that received equivalent fluences of nitrogen ions. Four data points were insufficient to determine if there was a trend in the change in carrier concentration after each irradiation; therefore, there is a fifth data point for sample 1200-2. (see Figure 36).

Sample 500-2

Due to the Hall system not being initially available, sample 500-2 was measured differently. Mobility and carrier concentration were measured only after the irradiation was finished. Initial post-irradiation Hall measurements resulted in a decrease in carrier concentration and a mobility that was higher than pre-irradiation values but decreased to less than pre-irradiation values. The sample was measured again approximately 5 ½ hours later. Mobility continued to decrease, while carrier concentration showed signs of recovery. The decrease in mobility indicates an increase in lattice atom displacements at or near the 2DEG creating scattering sites, which slow the electrons. Increases in carrier concentration can be attributed to positively charged defects in the AlGaN at the interface, which also correspond to negative shifts in V_{th} [4].

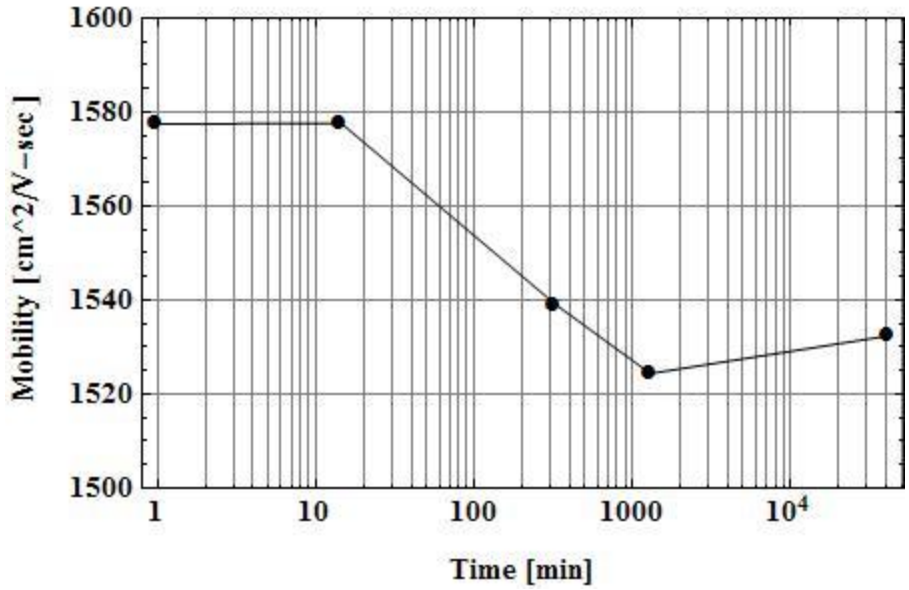

Figure 38. Average carrier mobility as a function of time for sample 500-2. Mobility decreases with time after irradiation but eventually recovers. Standard deviation was less than 1% except at 1300min where it was 12% of the average value.

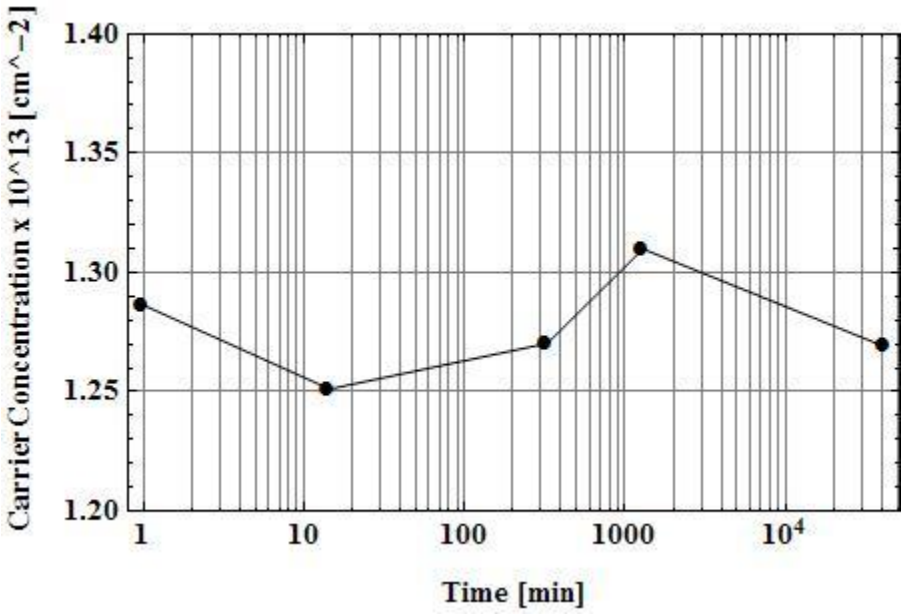

Figure 39. Average carrier mobility for sample 500-2 irradiated with 20 keV nitrogen ions normally incident to a fluence of about 9×10^{9} cm^{-2}. Carrier density is initially decreased but recovers over time. Standard deviation was less than 0.2% except at 1300 min where it was 6% of the average value.

Samples 0-2 and 500-3

The mobility of samples 0-2 and 500-3 decreased as a function of fluence. Carrier concentration in 500-3 decreased as a function of fluence but increased in 0-2. (Figure 40 and Figure 41). Hall measurement results for sample 0-2 was as expected; the mobility decreased with increasing fluence, while carrier concentration increased. Overall, the mobility decreased 38%, and carrier concentration increased 10% from pre-irradiation values. The decrease in mobility indicates an increase in lattice atom displacements at or near the 2DEG creating scattering sites which slow the electrons. The increase in carrier concentration in sample 0-2 can be attributed to positively charged defects in the AlGaN at the interface, which also correspond to negative shifts in V_{th} [4].

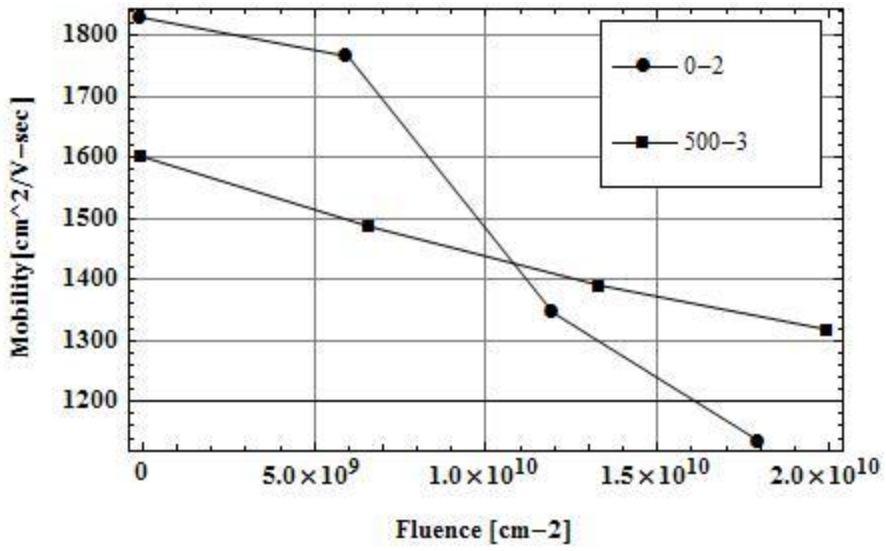

Figure 40. Carrier mobility as a function of fluence for samples 0-2 and 500-3. Carrier mobility for sample 0-2 decreased ~40% while it decreased only ~20% for sample 500-3.

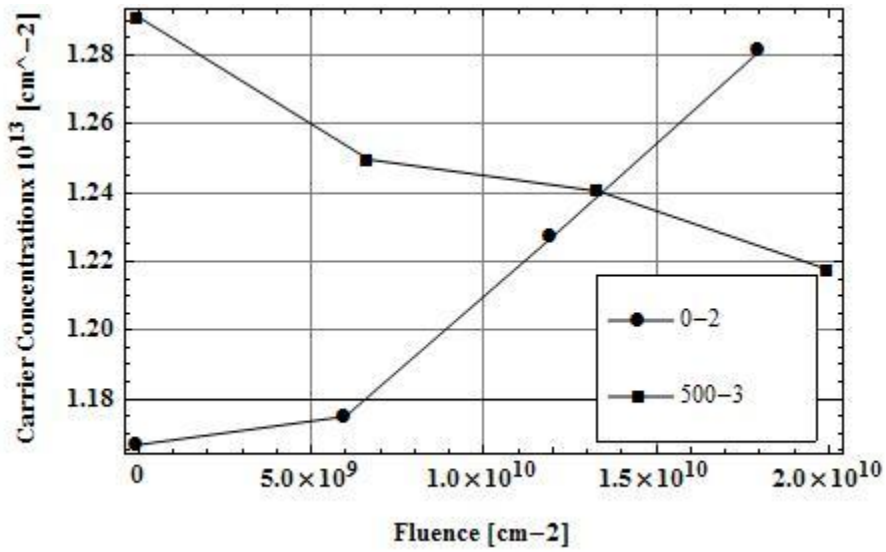

Figure 41. Carrier concentration as a function of fluence for sample 0-2 and 500-3. The carrier concentration for sample 0-2 increases 9% while for sample 500-3 it decreases about 4%.

Samples 200-2 and 1200-2

Sample 200-2 and 1200-2 showed much less change in mobility and carrier concentration. The mobility decreased as a function of fluence as shown in Figure 42.

Carrier concentration in sample 200-2 increased as a function of fluence while it decreased in sample 1200-2 as shown in Figure 43.

Sample 200-2 showed the least amount of change in Hall data. The mobility decreased about 1% while the carrier concentration may have slightly increased (less than 1%).

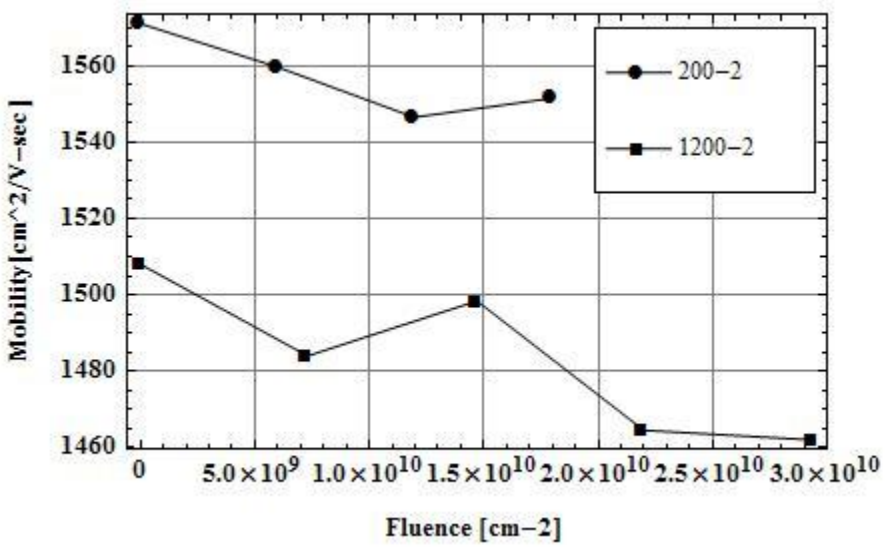

Figure 42. Mobility as a function of fluence for AlGaN/GaN structures passivated with 200 Å and 1200 Å Si_3N_4. Sample 200-2 was irradiated with 15 keV nitrogen ions at an incident angle of 45 degrees. Sample 1200-2 was irradiated with 50 keV nitrogen ions normally incident.

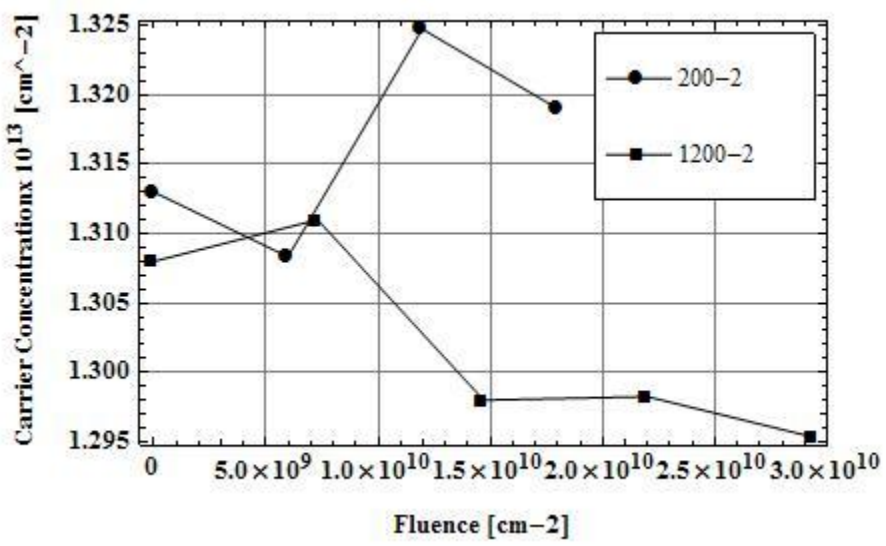

Figure 43. Carrier concentration as a function of fluence for AlGaN/GaN structures passivated with 200 Å and 1200 Å Si_3N_4. Sample 200-2 was irradiated with 15 keV nitrogen ions at an incident angle of 45 degrees. Sample 1200-2 was irradiated with 50 keV nitrogen ions normally incident.

A decrease in mobility indicates an increase in lattice atom displacements at or near the 2DEG creating scattering sites which slow the electrons. Changes in carrier concentration can be attributed to positively charged defects in the AlGaN at the interface, which also correspond to negative shifts in V_{th} [4].

V. Conclusions and Recommendations

Irradiation of passivated and unpassivated AlGaN/GaN structures by low energy nitrogen ions creates ionizing and displacement damage that affect capacitance, current, mobility, and carrier concentration in the 2DEG. C-V measurements yielded the most information compared to Hall measurements or at least in conjunction with Hall measurements, due to the significant shifts in capacitance after the Hall measurements were made.

The decrease in capacitance in the accumulation region C-V curves indicates an increase in the series resistance of the AlGaN following ion irradiation. According to [19], the "increase in capacitance in the inversion region indicates an increase in trapped positive charge in the AlGaN" attracting more electrons to the 2DEG. This corresponds to the increase in sheet carrier density in the unpassivated sample. However, the passivated samples experienced an increase in capacitance in the inversion region but a decrease in sheet carrier concentration. Additionally, roll-off of capacitance in the accumulation region also indicates series resistance in the AlGaN and/or Si_3N_4.

I-V measurements of the passivated samples after irradiation demonstrated behavior more consistent with Ohm's law than with the diode-like behavior of the Schottky junction prior to irradiation. This can be interpreted as leakage through the junction. In [11] and [15] it is argued that direct tunneling through the Schottky barrier is less likely than trap-assisted tunneling. "A low density of bulk traps distributed over the AlGaN layer causes a current by two-step tunneling via these traps" [15]. A greater density of radiation-induced damage sites (traps) would increase this tunneling mechanism.

There are many variables in this research that merit further investigation. Due to the variety of passivation thicknesses in addition to multiple fluences, there is a wide variety in the resulting data. Looking at each passivation thickness separately, particularly the 500 Å thickness, would allow a more in-depth analysis of the phenomena occurring due to the irradiation of the passivation layers. Other recommendations for further work include conducting C-t measurements as a function of fluence to determine if the capacitance would change the same way over time without the samples being exposed to magnetic fields as well as conducting C-V measurements during Hall measurements. Since Hall measurement magnet movement is manual, C-V could be measured in between and after the magnets are inserted to narrow down what effects the magnetic fields have on charge movement and thus capacitance. A more thorough investigation into I-V characteristics between -1 and 1 V would provide better insight into what is happening at the Schottky junction as a result of irradiation. Additionally a variety of spectroscopic methods could be applied to the irradiated samples to gather additional information about damage sites and the annealing process.

Appendix

0-2 20110112 Hall.txt

DATE	User_Name	Sample_Name
01-12-2011	RMay10	0-2Jan12

I(mA)	B	D	D_T	MN	T(K)
0.540	0.540	0.100	0.100	1000	300

n-type

Nb	u	rho	RH	RHA	RHB	NS	SIGMA	DELTA	ALPHA
-1.145E+18	1.749E+03	3.116E-03	-5.450E+00	-5.450E+00	-5.451E+00	-1.145E+13	3.209E+02	2.943E+01	9.486E-01

	Vab	Vbc	Vac	Vmac	V-mac	Vcd	Vda	Vbd	Vmbd	V-mbd
+I:	-36.133	-38.097	1.931	-13.916	17.868	-36.147	-38.114	1.934	17.868	-13.926
-I:	36.176	38.136	-1.980	13.963	-17.817	36.164	38.113	-1.984	-17.827	13.963

DATE	User_Name	Sample_Name
01-12-2011	RMay10	0-2Jan12

I(mA)	B	D	D_T	MN	T(K)
0.540	0.540	0.100	0.100	1000	300

Nb	u	rho	RH	RHA	RHB	NS	SIGMA	DELTA	ALPHA
-1.143E+18	1.751E+03	3.119E-03	-5.461E+00	-5.462E+00	-5.460E+00	-1.143E+13	3.206E+02	2.949E+01	9.488E-01

	Vab	Vbc	Vac	Vmac	V-mac	Vcd	Vda	Vbd	Vmbd	V-mbd
+I:	-36.173	-38.129	1.941	-13.959	17.893	-36.182	-38.144	1.901	17.899	-13.948
-I:	36.217	38.167	-1.997	14.017	-17.836	36.207	38.145	-1.954	-17.853	13.989

Figure 44. A print-out of Hall measurement data from the Ecopia HMS-3000 Hall Measurement System. The user can choose to save each data set separately or to append them in one file as shown here. The mobility and carrier concentration from the first data set were compared to calculations done using the Van der Pauw hall measurement worksheet (see Figure 45).

Bob Thurber connecting cables to the sample holder for a Hall effect measurement.

Contact
W. Robert Thurber
301-975-2067

100 Bureau Drive, MS 8120
Gaithersburg, MD 20899-8120

Sample Worksheet

SHARE

Van der Pauw Hall Measurement Worksheet

Sample Identification O-2 AlGaN/GaN
Thickness if known (cm) _____ Dimensions 5x5mm
Date 1/12/11 Lab 470 Operator RWT
Chemical Pretreatment (if any) _____
Contact Metal Al/Ti/Ni/ Contact Process _____
Comments All measurements in the dark

Resistivity Measurement

Temperature (°C or K) ~300K

	mA		mV		Ω
I_{21}	.54	V_{34}	36.147	$R_{21,34}$	66.94
I_{12}		V_{43}	36.164	$R_{12,43}$	66.97
I_{32}		V_{41}	38.114	$R_{32,41}$	70.58
I_{23}		V_{14}	38.113	$R_{23,14}$	70.58
I_{43}		V_{12}	36.113	$R_{43,12}$	66.89
I_{34}		V_{21}	36.176	$R_{34,21}$	66.99
I_{14}		V_{23}	38.097	$R_{14,23}$	70.55
I_{41}		V_{32}	38.136	$R_{41,32}$	70.62

Temperature ~300K

R_A = 66.95 (Eq. 10) R_B = 70.58 (Eq. 10)

$\exp(-\pi R_A/R_S) + \exp(-\pi R_B/R_S) = 1$
(Eq. 3, section IV algorithm, or see ASTM F76)

R_S = 311.6 Ω/□

For known thickness: $\rho = R_S d$ = _____ Ω-cm

Hall Voltage Measurement

Temperature (°C or K) ~300K

+B Field (G) 5400G

I_{13}	+.54	V_{24P}	17.868
I_{31}	-I_{13}	V_{42P}	-17.827
I_{42}	+	V_{13P}	-13.916
I_{24}	-I_{42}	V_{31P}	13.963

need to all be −

-B Field (G) 5400G

I_{13}	+.54	V_{24N}	-13.926
I_{31}	-	V_{42N}	13.963
I_{42}	+	V_{13N}	17.868
I_{24}	-	V_{31N}	-17.817

need to all be +

Temperature ~300K

$\Sigma V = -.127V$ n-type

ΣV_i (Eq. 11)

$n_S = 8\times10^{-8}\, I\, B / q|\Sigma V_i|$ (Eq. 12)

n_S = +1.143E13 cm^{-2}

For known thickness: $n = n_S / d$ = _____ cm^{-3}

$\mu = 1 / q\, n_S\, R_S$ = 1747 $cm^2\, V^{-1}\, s^{-1}$ (Eq. 2)

Figure 45. Van der Pauw hall measurement worksheet used to verify the data from the HMS-3000 Hall Measurement System from Ecopia. Instead of using I_{21}, I_{12}, etc., the Ecopia system uses +I and -I, so the signs from the Ecopia data sheets need to be adjusted as shown on this worksheet. For example, all the voltages for the +B field need to be negative, and all the voltages for the –B field need to be postitive to result in the correct ΣV_i.

Bibliography

[1] Kevin D. Greene, "Electron Paramagnetic Resonance Spectroscopy and Hall Effect Studies of the Effects of Low Energy Electron Irradiation on Gallium Nitride," Air Force Institute of Technology, PhD Dissertation 2003.

[2] Thomas E. Gray, "Investigation of Gate Current in Neutron Irradiated AlGaN/GaN Heterogeneous Field Effect Transistors Using Voltage and Temperature Dependence," Air Force Institute of Technology, Master Thesis 2007.

[3] Thomas D. Jarzen, "Capacitance-Voltage Study on the Effects of Low Energy Electron Radiation on AlGaN/GaN High Electron Mobility Transistors," Air Force Institute of Technology, Master Thesis 2005.

[4] J. W. McClory, J. C. Petrosky, J. Sattler, and T. Jarzen, "An Analysis of the Effects of Low-Energy Electron Irradiation of AlGaN/GaN HFETs," *IEEE Transactions on Nuclear Science*, vol. 54, no. 6, pp. 1946-1952, December 2007.

[5] Merrill Skolnik, *Radar Handbook*, 3rd ed.: McGraw Hill, 2008.

[6] J. W. McCLory, "The Effect of Radiation on the Electrical Properties of Alluminum Gallium Nitride/Gallium Nitride Heterostructures," Air Force Institute of Techonology, PhD Dissertation 2008.

[7] Ramakrishna Vetury, Naiqain Q. Zhang, Stacia Keller, and Umesh K. Mishra, "Impact of Surface States on the DC and RF Characteristics of AlGaN/GaN HFETs," *IEEE Transactions on Electrical Devices*, vol. 48, no. 3, pp. 560-566, March 2001.

[8] T. R. Prunty et al., "Passivation of AlGaN/GaN Heterostructures with Silicon Nitride for Insulated Gate Transistors," in *2000 IEEE/Cornell Conference onHigh Performance Devices*, Ithaca, NY, 2000, pp. 208-214.

[9] R. Gaska, J. W. Yang, A. Osinsky, A. D. Bykhovski, and M. S. Shur, "Piezoeffect and gate current in AlGaN/GaN high electron mobility transistors," *Applied Physics Letters*, vol. 71, no. 25, pp. 3673-3675, December 1997.

[10] Li Chengzhan et al., "Effect of Passivation on Increasing of AlGaN/GaN HEMT Gate Reverse Leakage," in *8th International Conference on Solid State and Integrated Circuit Technology*, Shanghai, 2006, pp. 908-910.

[11] James M. Sattler, "An Analysis of the Effects of Low Energy Electron Radiation on AlGaN/GaN Modulation-Doped Field-Effect Transistors," Air Force Institute of Technology, Master Thesis 2004.

[12] Daniel A. Roley, "Trap-Assisted Tunneling in AlGaN/GaN High Electron Mobility Transistors," Air Force Institute of Technology, Master Thesis 2006.

[13] D. Mahaveer Sathaiya and Shreepad Karmalkar, "Thermionic trap-assisted tunneling model and its application to leakage currents in nitrided oxides and AlGaN/GaN high electron mobility transistors," *Journal of Applied Physics*, vol. 99, no. 9, pp. 093701-1 - 093701-6, May 2006.

[14] Brad D. White et al., "Characterization of 1.8-MeV proton-irradiated AlGaN/GaN field-effect transistor structures by nanoscale depth-resolved luminescence spectroscopy," *IEEE Transactions on Nuclear Science*, pp. 2695-2701, Dec 2002.

[15] D. Mahaveer Sathaiya and Shreepad Karmalkar, "Edge Effects on Gate Tunneling Current in HEMTs," *IEEE Transactions on Electron Devices*, vol. 54, no. 10, pp. 2614-2622, Oct 2007.

[16] S. M. Sze, *Semiconductor Devices: Physics and TEchnology*, 2nd ed. United States of America: John Wiley & Sons, 2002.

[17] T. P. Ma and Paul V. Dressendorfer, Eds., *Ionizing Radiation Effects in MOS Devices and Circuits*. New York: John Wiley & Sons, 1989.

[18] Barton J. Gordon, "C-V Plotting: Myths and Methods," *Solid State Technology*, pp. 57-61, Jan 1993.

[19] Thomas D. Jarzen, "Capacitance-Voltage Study on the Effects of Low Energy Electron Radiation on AlGaN/GaN High Electron Mobility Transistors," Air Force Institute of Technology, Master Thesis 2005.

[20] E. F. Schubert. (2003) Rensselaer Department of Electrical, Computer, & Systems Engineering. [Online]. http://www.ecse.rpi.edu/~schubert/Course-ECSE-2210-Microelectronics-Technology-2003/MT-26-Ch16-3.pdf

[21] J. Schmitz et al., "The RF-CV method for characterization of leaky gate dielectrics," *Microelectronic Engineering*, vol. 72, no. 1-4, pp. 149-153, April 2004.

[22] W. Robert Thurber. (2010, April) NIST. [Online]. http://www.nist.gov/pml/semiconductor/hall_effect.cfm

[23] J. F. Ziegler, J. P. Biersack, and M. D. Ziegler, *SRIM: The Stopping and Range of Ions in Matter*. Morrisville, NC, U.S.A.: Lulu Press Co.

[24] S. R. Messenger et al., "Nonionizing Energy Loss (NIEL) for Heavy Ions," *IEEE Transactions on Nuclear Science*, vol. 46, no. 6, pp. 1595-1602, Dec 1999.

[25] Insoo Jun, Wousik Kim, and Robin Evans, "Electron Nonionizing Energy Loss for Device Applications," *IEEE Transactions on Nuclear Science*, vol. 56, no. 6, pp. 3229-3235, Dec 2009.

[26] Bart Van Zeghbroeck, *Principles of Semiconductor Devices*. Boulder, CO: University of Colorado, 2007.

[27] Hang-Ting Lue, Chih-Yi Liu, and Tseung-Yuen Tseng, "An Improved Two-Frequency Method of Capacitance Measurement for SrTiO3 as High-k Gate Dielectric," *IEEE Electron Device Letters*, vol. 23, no. 9, pp. 553-555, September 2002.

[28] Carl Scharrer and Yuegang Zhao. ElectroIQ.com. [Online]. http://www.electroiq.com/index/display/semiconductors-article-display/199088/articles/solid-state-technology/volume-47/issue-2/features/metrology/high-frequency-capacitance-measurements-monitor-eot-of-thin-gate-dielectrics.html

[29] E. H. Nicollian and J. R. Brews, *MOS (Metal Oxide Semiconductor) Physics and Technology*, Wiley Classics Library Edition ed. Hoboken, USA: John Wiley and Sons, Inc., 2003.

[30] S. R. Messenger et al., "Nonionizing Energy Loss (NIEL) for Heavy Ions," *IEEE Transactions on Nuclear Science*, vol. 46, no. 6, pp. 1595-1602, December 1999.

REPORT DOCUMENTATION PAGE

Form Approved
OMB No. 074-0188

1. REPORT DATE *(DD-MM-YYYY)*	**2. REPORT TYPE**	**3. DATES COVERED** *(From – To)*
24-03-2011	Master's Thesis	Jun 2010 – Mar 2011

4. TITLE AND SUBTITLE

Investigation of Gate Leakage Current in Nitrogen-Irradiated AlGaN/GaN Heterostructures

5a. CONTRACT NUMBER

5b. GRANT NUMBER

5c. PROGRAM ELEMENT NUMBER

6. AUTHOR(S)

May, Rose E., Captain, USAF

5d. PROJECT NUMBER

5e. TASK NUMBER

5f. WORK UNIT NUMBER

7. PERFORMING ORGANIZATION NAMES(S) AND ADDRESS(S)
Air Force Institute of Technology
Graduate School of Engineering and Management (AFIT/EN)
2950 Hobson Way
WPAFB OH 45433-7765

8. PERFORMING ORGANIZATION REPORT NUMBER
AFIT/GNE/ENP/11-M14

9. SPONSORING/MONITORING AGENCY NAME(S) AND ADDRESS(ES)
National Nuclear Security Agency
Attention: Maj. Paul Adamson
US Department of Energy NA-10 Defense Programs
1000 Independence Ave.
Washington, DC 20585

10. SPONSOR/MONITOR'S ACRONYM(S)

11. SPONSOR/MONITOR'S REPORT NUMBER(S)

12. DISTRIBUTION/AVAILABILITY STATEMENT
APPROVED FOR PUBLIC RELEASE; DISTRIBUTION UNLIMITED

13. SUPPLEMENTARY NOTES

14. ABSTRACT
Due to commercial and government interest in devices capable of functioning in high-power, high-frequency space applications, radiation tolerant AlGaN/GaN devices have been under study in recent years. Passivation of the AlGaN surface by (Si_3N_4) prevents electron trapping and enhances the 2DEG, but it also increases gate leakage currents, which can lead to device failure. This study sought information about current leakage mechanisms by introducing displacement damage close to the Si_3N_4/AlGaN interface. The effects of irradiation damage around the Si_3N_4/AlGaN interface on irradiation-induced leakage current were investigated for three thicknesses of a Si_3N_4 passivation layer in addition to an unpassivated sample. AlGaN/GaN samples were irradiated at room temperature with 15-50keV nitrogen ions. Hall measurements determined mobility and 2DEG carrier density. C-V measurements provided insight into charge location and effects of the band structure. Pre-irradiation measurements were compared to the irradiation results to determine the types and amounts of damage done in the devices. Post-irradiation C-V measurements showed greater than 50% decrease in capacitance and an average -3V shift in V_{th} which persisted in the passivated samples. Post-irradiation Hall measurements showed decreases in mobility for both passivated and unpassivated samples. Carrier concentration decreased for passivated samples but increased for the unpassivated sample.

15. SUBJECT TERMS
AlGaN/GaN, heterostructure, gate leakage current, silicon nitride, passivation

16. SECURITY CLASSIFICATION OF:			**17. LIMITATION OF ABSTRACT**	**18. NUMBER OF PAGES**	**19a. NAME OF RESPONSIBLE PERSON**
a. REPORT	**b. ABSTRACT**	**c. THIS PAGE**			James C. Petrosky (AFIT/ENP)
U	U	**U**	**UU**	73	**19b. TELEPHONE NUMBER** *(Include area code)* 937-255-3636 ext. 4562

Standard Form 298 (Rev. 8-98)
Prescribed by ANSI Std. Z39-18